University of Mohamed Kheider of Biskra
Exact Sciences and Sciences of Nature and Life Matter Sciences
Department of Material Sciences

Final Dissertation in Master

Field of Material Sciences
Physics Stream
MaterialsPhysics Specialty
Ref. : Entrez la référence du document

Presented by:
TounsiAssia

The: Monday 28/09/ 2020

Temperature effect on the performance of Cu(In,Ga)Se₂ (CIGS)- based solar cell

Jury :

OuahabA.Ouahab	Professor	Med KhiderUniversity- Biskra	President
MeftahAmjad	Professor	Med KhiderUniversity- Biskra	Supervisor
Marmi Saida	M.C.B	Med KhiderUniversity- Biskra	Examiner

Academic Year:2019/2020

<u>Acknowledgement</u>

<u>Dedication</u>

This work is dedicated:

To my dear parents who supported, encouraged

loved me throughout my life,

to all my relatives and friends,

and finally to you , dearest reader

Abstract

In this work, we haves studied a Cu(In, Ga)Se_2 (CIGS) –based solar cell under the effect of the ambient temperature change in the range of [230°K-350°K]. The cell is exposed to theAM1.5 standard spectrum, and its performance was simulatedbySILVACO-ATLAS software, which allowed the calculation of both the internal and external parameters. These latter arerepresented by the currentdensity-voltage $(J-V)$ characteristic, from which wehave extracted the output photovoltaic parameterscharacterisingthe cell performance. The temperature, in general, has a slight effect on the internal parameterdistributions of the solar cell when these latter are calculatedunder the short circuit conditions.However, the temperature has a noticeable effect on the open circuit voltage V_{OC} which decreases significantly with temperature increase in the range [230°K-350°K]. This leads directly to the decrease of the fill factor FF, and consequently the decrease of the photovoltaic conversion efficiency η from 22.31% for 230°K to 13.52% for350°K.

List of Figures

List of Tables

List of symbols

Symbol	Definition	Unit
E	Photon energy	eV
Λ	Wavelength	M
I_s	the diode saturation current	A
Q	elementary charge	C
V	the voltage of the cell	V
K	Boltzmann constant	J/K
T	Absolutetemperature	K
I_L	the photo generationcurrent	A
I_{oc}	the open circuit current	A
E_g	band-gap energy of the semiconductor	eV
N_C	Density of states in conduction band	cm^{-3}
N_V	Density of states in valence band	cm^{-3}
N_A	Acceptor doping	cm^{-3}
N_D	Donor doping	cm^{-3}
D_n	Electron diffusion constant	cm^2/S
D_p	Hole diffusion constant	cm^2/S
τ_n	Electron life time	S^{-1}
τ_p	Hole life time	S^{-1}

G	the generation rate	$cm^{-3}S^{-1}$
L	the diffusion length	m
R_L	Loadresistance	Ω
η	Conversion efficiency	%
P_{out}	the maximum output power	mW.cm^{-2}
P_{in}	the input power	mW.cm^{-2}
V_{mp}	the maximum power point voltage	V
I_{mp}	the maximum power current	A
FF	Fill factor	%
n	the refractive index	-
α	the absorption coefficient	cm^{-3}
D	Cellthickness	μm
x_{tot}	Cellwide	μm
ε_r	Permittivity	V/cm
χ	Affinity	eV
μ_n	Electron mobility	$cm^2V^{-1}s^{-1}$
μ_p	Hole mobility	$cm^2V^{-1}s^{-1}$

E_C	Conduction band energyedge	eV
E_V	Valence band energyedge	eV
E_{fn}	Quasi-Fermi level of electrons	eV
E_{fp}	Quasi –Fermi level of holes	eV
J_s	the saturation current density	mA.cm^{-2}
J_{ph}	Density of the photo-generated current in solar cell	mA.cm^{-2}
n_i	the intrinsic concentration	cm^{-3}
m_e^* , m_t^*	the effective masses of the electrons and holes.	Kg

Table of contents

Chapter I: Generalities around solar cells

Chapter II: CIGS based solar cells

General introduction

SolarcellwithCu(In,Ga)$\boldsymbol{Se_2}$ (CIGS) chalcopyrite semiconducting compound as an absorber are amongthin film devices ofhighestphotovoltaicefficiency, whichcurrentlyis close to 20 % forlaboratorycells [4,5]. The successful development of this technology aboutfundamental properties of CIGS compounds, especially about defectscontrolling photovoltaic performance of these device, and used an absorberlayer for the incoming light, and Cadmium Sulfide (CdS), which has the mainfunction of the buffer layer is to be a good hetero-junction partner to the p-type absorber layer with minimal lattice mismatch to minimize defects likeinterface states and be transparent to incident light [5]. The window layerstransmit most of the light from the solar spectrum owing to their large bandgaps, for the n-type partner in the junction, which at the same time needsto be sufficiently conductive to serve as front contact, ZnO is cheap andrather easy to grow, making it the general choice [7].

In this study, we investigate the performance of a Cu(In,Ga)Se$_2$ (CIGS)-based solar cell, achieved by the SILVACO-ATLAS numerical simulation software, which allows the computation ofall the internal parametersof the solar cell such as the distribution of the energy band diagram, electron and hole concentrations, the recombination rate, as well as the external parameters represented by the current density-voltage$(J - V)$ characteristic, through which the output photovoltaic parameters characterizing the cell performance can be extracted, namely the short circuit current density J_{sc}, the open circuit voltage V_{oc}, the fill factor FF, the maximum power P_{max} providedby the cell and the photovoltaic conversion efficiencyη of the solarcell. The aim of this work is to study the effect of the ambient temperature on the performance of the CIGS-basedsolar cell exposed to AM1.5 standard solar spectrum in terms of the temperature effect on both internal and externalparameters. The consideredtemperature range is [230°K-350°K] equivalent to [(-43°C)-(77°C)]. The solar cellmay be exposedto the low temperature, for example, through the climatic conditions of cold regions.The solar cell may be exposed to high temperature, for example, when it is continuously exposed to solar radiation in hot regions.

In addition to the general introduction and conclusion, our thesis will be organized as follow:

In the first chapter, we will talkabout the solar spectrum and energy,the photo-generationprocess of electron-holepairs, the solar cell current-voltage characteristics, the

non-ideal factors in solar cell characteristics, and finally an overview of the current commercial technologiesis presented.

In the second chapter we will talk about the $Cu(InGa)Se_2(CIGS)$-based solar cells and thedevice physics.

In the third chapter we will talk about Silvaco-Atlas as the simulation used software and the device basic construction layout.

In the fourth chapter,we will presenta detaileddescription of the studied CIGS-based solar cell, and we will give and discusstheresults obtained by our simulation using Silvaco-Atlas software.

Chapter I:

Generalities around solar cells

I.1.Introduction:

Solar cells are semiconductor devices that rely on the absorption of light, specifically photons, from the solar spectrum to generate electron-hole pairs. The separation and subsequent collection of these electron-hole pairs is the method by which solar cells convert solar energy into useful electricity. In order to create a new solar cell design, a thorough understanding of the underlying science and physics is a requirement.

In this first chapter, we first present some concepts related to solar spectrum and wavelength energy, photo generation of electron hole pairs, and solar cell current voltage characteristics, then we will cite an overview of current commercial technologies.

.I.2.Solar Spectrum and Wavelength Energy:

There are multiple standard spectrum classifications used in the study of solar cells. The first, AM0, is the solar spectrum observed in space. It has the widest range of wavelengths and contains approximately 1.4 kW per meter squared (kW/m^2) of solar energy available for absorption [1]. When examining terrestrial applications of solar cells, AM1.5 is the predominant standard used for analysis and simulation. It has a slightly different profile than AM0, (Figure I).
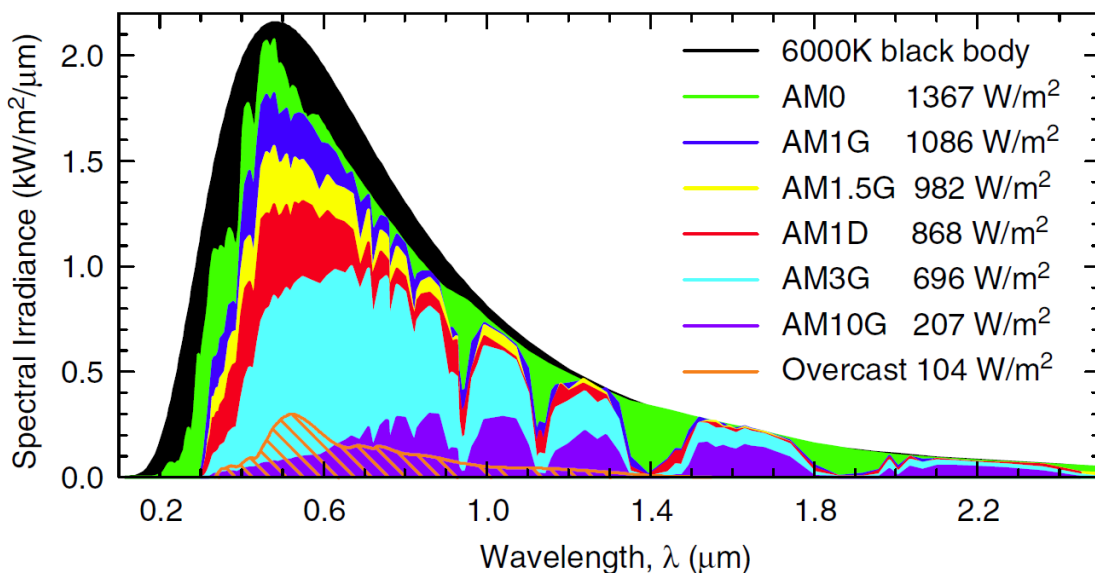
Figure I.1: Solar irradiance spectrum breakdowns for various classifications [2].

Most of the differences between the spectra are a result of water present in the atmosphere that absorbs some of the available photons as they radiate to the Earth'ssurface. The result is fewer photons available for solar cells to convert to usable

energy, a reduction to approximately 1 kW/m^2 [1]. Given a fixed amount of input energy, this makes the advancement of solar cells that increase efficiency or take advantage of a larger percentage of these photons necessary.

Once the solar spectrum is understood, the characteristics of photons must be considered. The most important photon characteristic is the wavelength of the photon. Each wavelength corresponds to a specific energy possessed by a given photon. This relationship is demonstrated by

$$E = \frac{1.24}{\lambda} \qquad\qquad (I.1)$$

Where E is energy in electron volts and λ is wavelength in micrometers.

From Equation (I.1), we see that longer wavelength photons contain less energy relative to shorter wavelength photons. Furthermore, photons of longer wavelengths have the ability to penetrate further into a solar cell than those with shorter wavelength. This must be considered when constructing solar cells that have the ability to absorb photons with varying energy levels, such as multi-junction solar cells or graded band-gap solar cells.

I.3.Photogeneration of Electron Hole Pairs:

In order to create an electron-hole pair to generate power, a photon must displace a valence electron from a bond inside of the crystalline structure of the solar cell. The energy required to create these electron-hole pairs are determined by the band gap of the semiconductor absorber material. If the photon's energy is less than the band gap of the absorber, it is unable to generate an electron-hole pair and either passes through the material or is absorbed as heat. If the photon has energy higher than the band gap, it may generate an electron-hole pair, but the additional energy beyond the band gap is eventually dissipated as heat within the solar cell as the electron settles back to the conduction band. Photo generationisillustrated (Figure I.2).
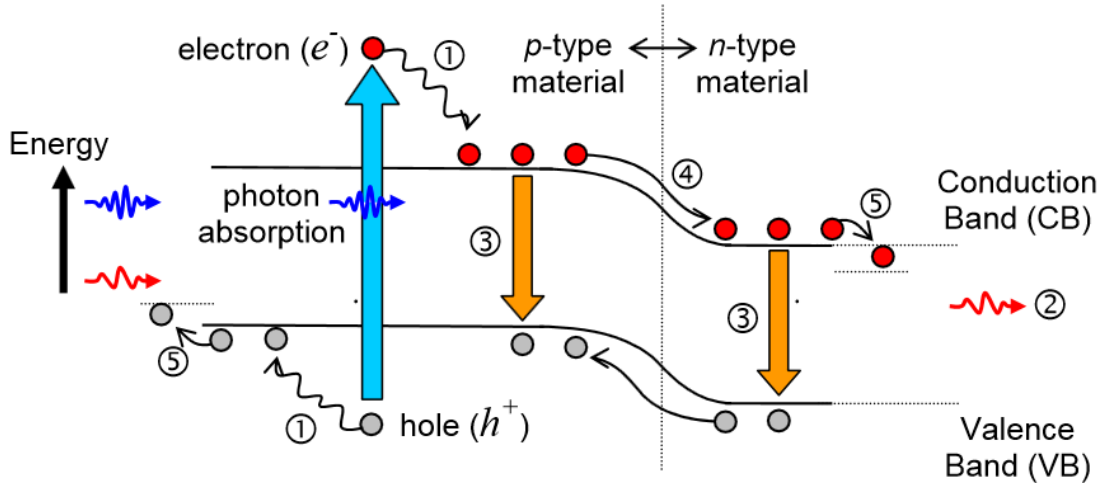
Figure I.2: Illustration of photo generation and recombination [2].

Once an electron-hole pair is created, it is necessary to move these individual carriers to one of the two contacts on the solar cell in order to harvest them before recombination can occur. The electric field that exists within the materials and junctions helps to sweep these carriers away from each other and towards the contact.

I.4.Solar Cell Current Voltage Characteristics:

There are several important physical principles behind the function of solar cells that are important to understanding how and why they work. The result of the photo generation caused by exposure of solar cells to sunlight is the creation of a voltage potential and a current within the cell. A solar cell is much like a diode as upon exposure to light it conducts in one particular direction, and when the exposure ceases, the diode stops conducting. These voltage and current responses of solar cells are guided by characteristics of each individual solar cell.

I.4.1.Short-Circuit Current:

The current in a solar cell is determined by several factors and the ideal current I expression is expressed by [13]

$$\text{I}= I_s(e^{\frac{qV}{KT}}\text{-1})\text{-}I_L \qquad\qquad\qquad (I.2)$$

Where I_s is the diode saturation current, q is charge, V is the voltage of the cell, k is Boltzmann's constant, T is temperature and I_L is the photo generation current. FromEquation (I.2), it can be seen that the open circuit current I_{OC} is equal to I_L since the exponential term becomes zero when there is no voltage across the device [3].

5

Expanding on Equation (2), the saturation current density J_s can be expressed by[3]

$$J_S = qN_C N_V \left(\frac{1}{N_A} \sqrt{\frac{D_n}{\tau_n}} + \frac{1}{N_D} \sqrt{\frac{D_P}{\tau_P}} \right) . e^{\frac{-Eg}{KT}} \tag{I.3}$$

Where the variables for Equation $(I.3)$ are defined in Table I.1

Table I.1: Variable definitions for current density equation.

Variable	Definition
E_g	Bandgap
N_C	Density of states in conduction band
N_V	Density of states in valence band
N_A	Acceptor doping
N_D	Donor doping
D_n	Electron diffusion constant
D_p	Hole diffusion constant
τ_n	Electron life time
τ_p	Hole life time

Typically, I_L is significantly larger than I_S and plays a much larger role in characterizing a solar cell. The photo generation current density J_L is [4]

$$J_L = qG (L_n + W + L_p) \tag{I.4}$$

Where G is the generation rate, L is the diffusion length, and W is the depletion width. The generation rate is determined by the intensity of the illumination that the solar cell is exposed to. The diffusion lengths L can be further defined by

$$L_n = \sqrt{D_n \tau_n} \tag{I.5}$$

And

$$L_p = \sqrt{D_p \tau_p} \tag{I.6}$$

From Equations (I.5) and (I.6), it can be seen that with a longer carrier lifetime and, therefore, longer diffusion length, the photo generation current is increased.

I.4.2.Open-Circuit Voltage:

After a thorough analysis of the current, the voltage V in a solar cell is determined by [3]

$$I = \frac{-V}{R_L} \qquad (I.7)$$

Where R_L is load resistance applied to the output of the solar cell. Guided by this relationship, Equation (I.2) can be solved for voltage when the current is equal to zero, which results in the open circuit voltage V_{oc} being expressed as [3]

$$V_{OC} = \frac{KT}{q}(\frac{I_L}{I_S}+1) \qquad (I.8)$$

I.4.3.Solar Cell Characteristics:

When conducting simulations and measurements of solar cells, the desired outputs are the current-voltage (IV) characteristics of the anode voltage of the device versus the cathode current. The effective photo generation of power is demonstrated by a significantly larger area under the curve when compared to non-illuminated conditions. This is typically completed by sweeping the anode voltage from zero volts to a predetermined maximum voltage. This maximum voltage varies between solar cells and is determined by the properties of the semiconductor materials that make up the cell. This curve demonstrates the behavior of the cell as it operates from its short circuit current to its open circuit voltage as demonstrated (Figure I.3).

From the IV curve, there are two important factors that are typically calculated. Once the curve has been produced, the efficiency η is calculated

$$\eta = \frac{P_{out}}{P_{in}} \qquad (I.9)$$

Where P_{out} is the maximumoutput power and P_{in} is the input power. The input power is determined by the area of the solar cell and the solar spectrum to which it is exposed. The maximum power is taken from the "knee" of the IV curve, where the product of the current and voltage is maximized as demonstrated (Figure I.3). The output power iscalculated from $P_{out} = V_{mp} I_{mp}$ where V_{mp} is the maximum power point voltage and I_{mp} is the maximum power current.
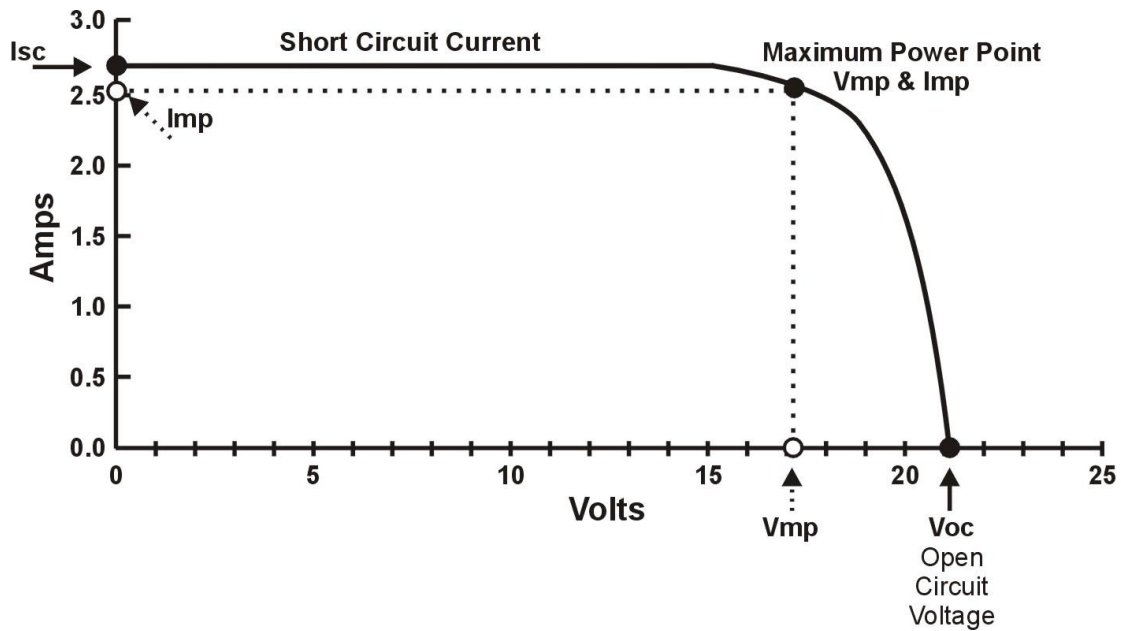
Figure I.3: Sample solar cell IV curve [5].

The second factor that is typically measured and reported is the fill factor. The fill factor *FF* is calculated from

$$FF = \frac{V_{mp}\, I_{mp}}{V_{oc}\, I_{sc}} \qquad\qquad (I.10)$$

Fill factor can be a maximum of 100%, and reductions are from a result of internal characteristics of the cell. The higher the fill factor, the more these internal factors have been reduced and the sharper the IV curve appears.

I.5. Non-ideal Factors in Solar Cell Characteristics:

There are several other factors that play a role in the performance of a solar cell that require discussion to ensure a thorough analysis.

I.5.1.Trap Assisted Recombination:

Recombination occurs when an electron from the conduction band and a hole from the valence band recombine, reducing the number of free carriers available within the semiconductor. This is especially detractive for solar cells because it reduces the number of carriers that can be harvested and turned into useful energy. Defects in solar cell materials can lead to traps which serve as recombination centers that reduce the output of the cell. Traps have an associated energy which dictates a forbidden energy level between the conduction band and the valence band where the carriers can be trapped. In addition, traps have a cross-sectional area where a higher value results in a higher probability of trapping

a carrier. Finally, trap density plays a large role in the recombination rate since carrier lifetime decreases as trap density increases. Trap assisted recombination is illustrated (figure I.4).
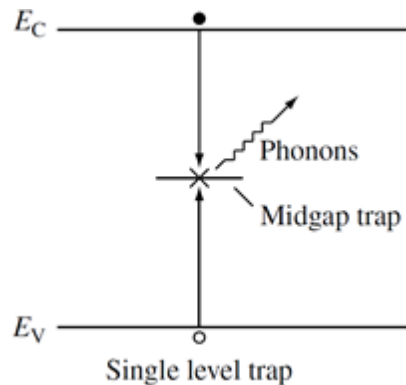
Figure I.4: Illustration of defect trap recombination process[6].

I.5.2.Contact Shading:

In order to harvest the electron-hole pairs generated by the photons absorbed in the solar cells, top and bottom contacts must be included. The bottom contact serves as the anode and can also serve to reflect photons that have penetrated all the way through the absorber layer to increase the output of the cell. The bottom contact typically does not detract from the performance of the solar cell.

The top contact serves as the cathode and is placed on top of the cell. The placement of a metal top contact, which reflects rather than passes photons, creates shading of the solar cell and has a significant impact on the output of the cell [7]. This results in a desire to reduce the area which is covered by the top contact, but a reduced coverage of top contacts results in a reduced ability to collect carriers.

In an attempt to reduce the shading, a thinner metal contact can be used, but the reduction in cross-sectional area increases the resistance of the top contact grid, effectively reducing the overall output of the cell more than the shading resulting from the top contacts. This requires the balancing of all of these factors to maximize the output of the cell. Overall, an estimated 10% of the top area of a cell is covered by a top grid that results in shading in order to efficiently harvest the energy created by the solar cell [7].

I.5.3.Temperature effects:

Temperature plays a large role in the output of a solar cell. For nearly all research, attempts are made in simulations and testing to hold the cell temperature at 25°C. While this makes it easy to conduct a comparison between solar cells, it creates an unrealistic

expectation of true device performance. As a result of being exposed to the sun and the absorption of photons, the operating temperature of solar cells increases during exposure. Typical uncooled solar cells tend to operate at temperatures near 50°C; though the actual operating temperature depends on several factors, including ambient temperature, wind speed, etc. This increase in temperature results in a decrease in the output voltage of the solar cell. This results in an output voltage decrease of 2.0 mV per degree [8], meaning that a solar cell operating at 50°C vice 25°C has a resulting 50.0 mV output voltage decrease. This decrease in output voltage can result in up to a 10% decrease in the output of the cell resulting from the higher operating temperature[9], [10].

I.5.4.Back Surface Field:

As discussed earlier, recombination plays a large role in the reduction of solar cell output and efficiency. Recombination occurs throughout the solar cell, with significant recombination sites being located at the top and bottom contacts of the cell. Some of this recombination can be reduced through the creation of a back surface field within the solar cell. A back surface field can be created by increasing the doping near the back contact. The back surface field serves to create an additional small electric field that helps to separate carriers, allowing for their collection and reducing recombination at the back contact[11], [12], [13].

I.5.5.Other Factors that Degrade Performance:

Reflection off of the top surface of the solar cell is another cause for degraded performance of solar cells. There has been much research on this topic, and it is standard for solar cells to be manufactured with an anti-reflective coating that reduces the number of photons that are reflected, resulting in the increased performance of the cell.

Another significant factor is the internal resistance of the cell. Since the cell is constructed of several different layers, each with its own electrical properties, the layers combine to create an internal resistance to the flow of electricity. Contributing factors include the ohmic contact between semiconductors and metal contacts, and the equivalent resistance of the contacts as well as the inherent resistance associated with the semiconductor materials used in the device.

I.6.An overview of current commercial technologies:

Although the global market was dominated by the first-generation panels that utilize crystalline silicon (c-Si) as the light absorbing constituent, there are different solar cell

technologies that have been developed based on different light absorbing materials and deployed commercially the world over. Figure I.5 shows a schematic of the most typical cell wherein the p-n junction is formed by doping the intrinsic silicon block (typically 180-200μm thick) with boron (to form the p-type layer) and phosphorous (to form the n-type layer), and joining the two layers together with their respective contacts [14]. The silicon used in these cells may be mono crystalline or multi crystalline, with the former providing higher efficiencies due to their lower concentration of defects and other impurities that can increase the material's internal resistance.

However, the fastest growing PV technology is the second generation of solar cells that utilize thin films (2-5μm) of CdTe or Cu-In-Ga-S,Se (CIGS) as the light absorbing constituent. (Figure I.6) is a representation of the two devices that are typically built in the superstrate and substrate configurations, respectively. Note that the core junctions in the two stacks are the ones formed between the p-type absorber (CdTe or CIGS) and n-type "window" material (CdS) that is transparent to the light radiation (incident from the top in both cases). The TCO materials that also serve as ohmic contacts to electron transport are cadmium stannate in CdTe and ITO (In2O3-SnO2 alloy) in CIGS. The hole contacts to the absorbers at the opposite end (to electron collection) of the two devices are copper and molybdenum.
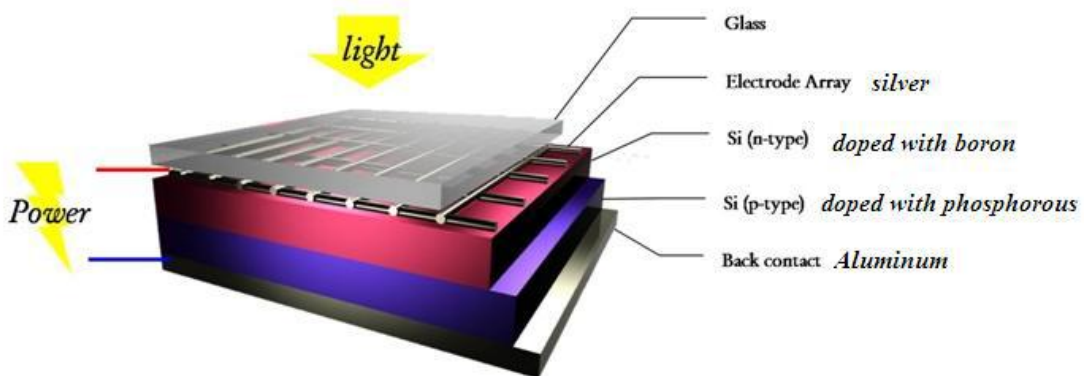
Figure I.5: The typical crystalline Si solar cell based on p-n junction [15].
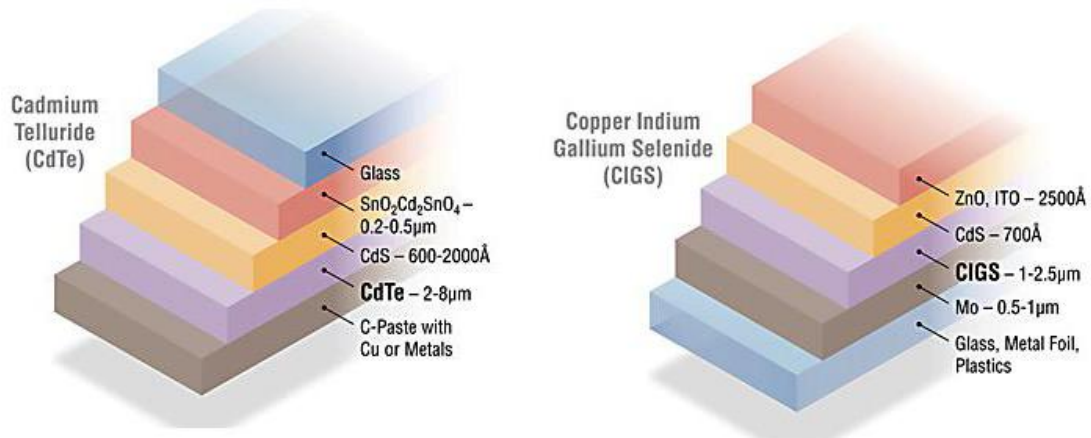
Figure I.6: Schematic illustrations of typical CdTe (left) and CIGS (right) PV devices [16].

The reasons for the much higher penetration rates of c-Si in the PV market are its much earlier maturation periods (1970s) compared to the thin films, which have been commercialized only in the past 5 years or so. The silicon cells typically also have higher efficiencies (25% [17]; mono-Si) compared to the record champion cell efficiencies for CdTe (17.3% [17]) or CIGS (20.3% [17]) devices. Current research efforts in the field of PV are heavily invested in improving the performance of the thin film technologies so that solar electricity can increasingly be an environmentally cleaner and more sustainable energy option

I.7.conclution:

In this first chapter, we have presented general concepts related to solar cells, such as the wavelength energy of the solar spectrum and the current voltage characteristics of solar cells, then an overview of the current commercial technologies was presented.

Chapter II:

CIGS based solar cell

II.1.Introduction:

It is customary for a solar cell to be named after its absorber material. CIGS is shorthand for Cu(In,Ga)Se_2, which has the chalcopyrite lattice structure, a direct bandgap, and can be, for the solar cells, in mono or polycrystalline natures.

In this chapter we will give an overview of the CIGS-based solar cell and the role of the different layersin its structure n-ZnO/n-CdS/p-Cu(In,Ga)Se_2 .The Developments in CIGS solar cell design, as well as the trap density in CIGS alloys and the device physics will also be presented.

II.2.Cu(InGa)Se_2 solar cells:

Cu(InGa)Se_2 is an alloy of copper indium diselenide (CuInSe_2) and copper gallium diselenide (CuGaSe2) which results in a material with characteristics interpolated between both components. The resulting material has a tunable bandgap depending on the mole fraction of Ga, where the mole fraction is calculated from

$$x = \frac{Ga}{Ga+In}$$

(II.1)

Where *Ga*is the mole fraction of gallium and *In*is the mole fraction of indium. The bandgap*Eg*ranges from 1.01 eV to 1.64 eV as the Ga mole fraction is increased from zero to one following [6]

$$Eg = 1.010 + 0.626x - 0.167x(1 - x)$$ (II.2)

Traditionally, with silicon solar cells, a homojunction is formed at the border between the *n*-type and *p*-type portions of the semiconductor. Cu(InGa)Se_2solar cell do not form a homojunction but rather a heterojunction as a result of the differences in electrical properties between the materials. Specifically, due to the differences in bandgaps of the two materials that form a junction, discontinuities in the band diagrams occur which may create barriers to the flow of carriers [6].

II.2.1.n-CdS/Cu(InGa)Se_2 Solar Cell design:

Much like other solar cells, the standard Cu(InGa)Se_2 cell follows traditional structure designs containing a top contact, a window layer, a buffer layer, an absorber layer, a back contact layer, and the substrate in which it is placed. The standard structural layout of a

$Cu(InGa)Se_2$ cell is illustrated (Figure II.1). Additionally, a cutline from the top of the cell to the bottom provides a band-structure diagram as demonstrated (Figure II.2).
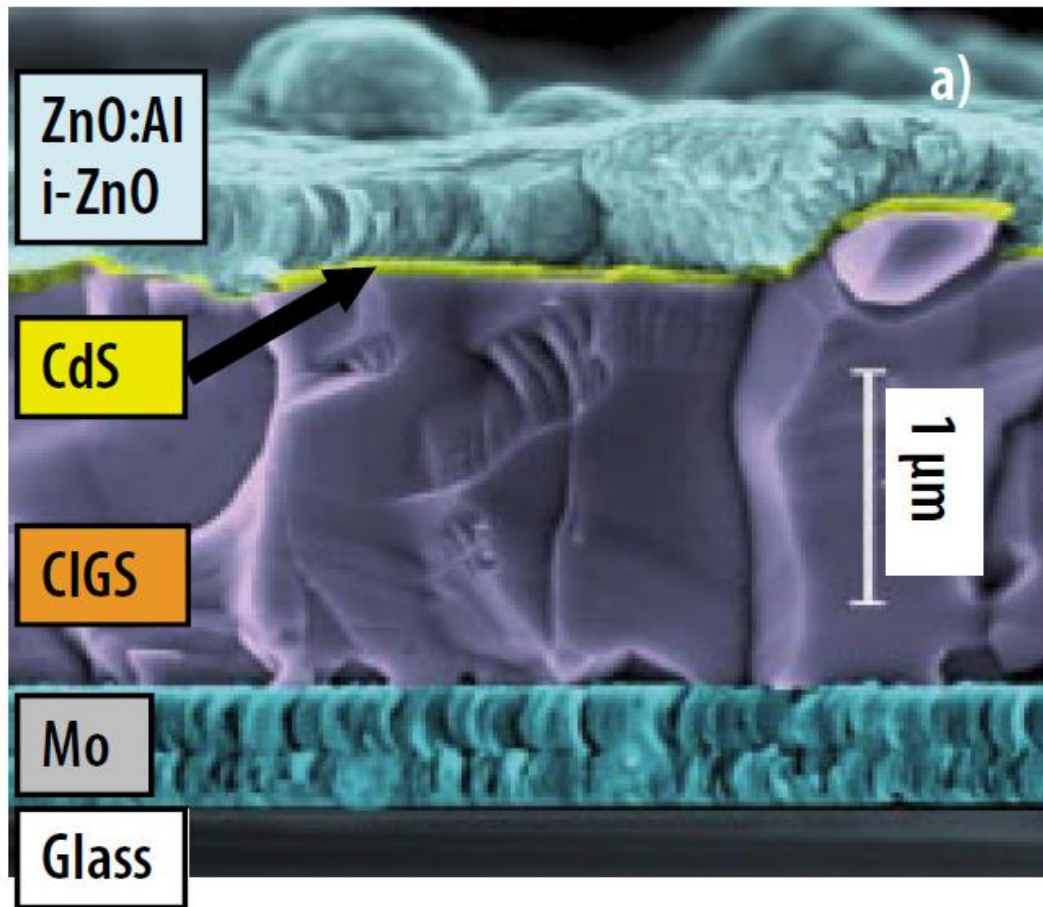
Figure II.1: Colorized scanning electron microscope image of $Cu(InGa)Se_2$ structur [18].

There are several substrate options for the $Cu(InGa)Se_2$ solar cells, with the most popular options being soda lime glass and thin metal films. Soda lime glass is a rigid structure but has been used in most of the research due to the simplicity and stability of its application as well as its low cost. Thin film metal substrates are used less often but have the largest upside future for commercial production. The thin film metal substrate is both lighter and more flexible than the soda lime glass but come with a higher relative cost.
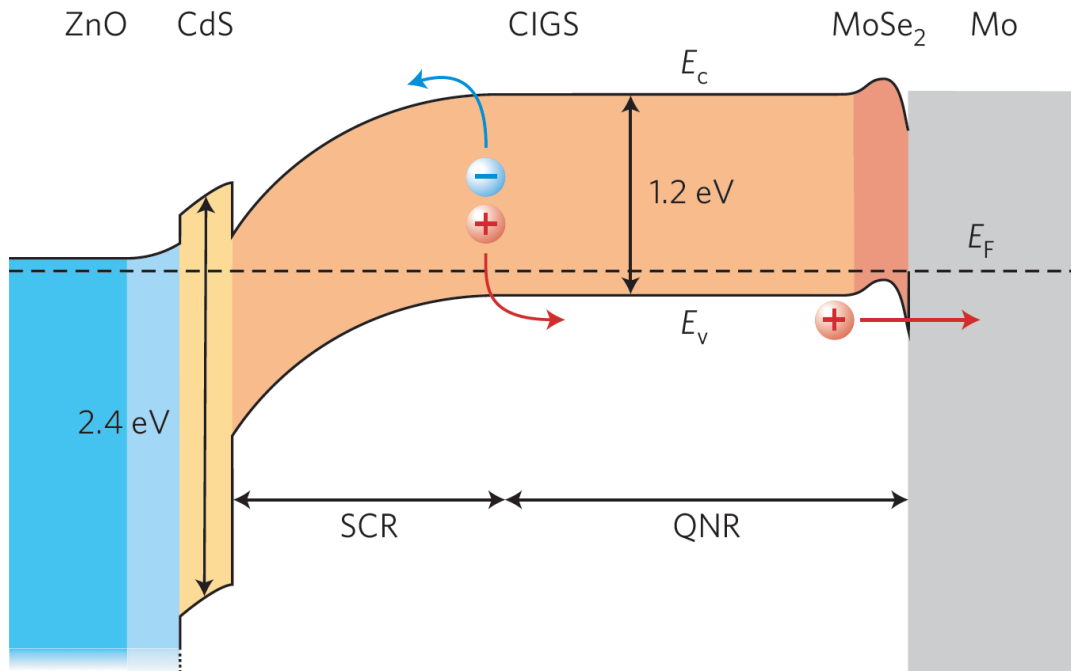
Figure II.2: Band structure for Cu(InGa)Se_2 solar cell [19].

The next layer above the substrate in the cell is the molybdenum (Mo) back. This layer serves to not only as the bottom contact but also as part of the substrate. Several materials have been investigated, but Mo has been shown to be the best choice as it demonstrates low electrical resistance, is resistive to Cu and In permeation, and is stable at temperatures required for processing [20].

The third layer is the *p*-type Cu(InGa)Se_2 absorber. The primary difference observed between absorber layers in different designs is the Ga concentration as a result of the tunable bandgap. Furthermore, the thickness of the absorber layer varies significantly between cells. While it is important to keep the absorber layer thin to maintain the cell's flexibility, it is a widely studied parameter. Ultra-thin CIGS absorber layers have been studied and efficiencies have been simulated to be in the 10–11% range but have not been widely produced [21]. Thicker layers have also been studied, but thicknesses is typically limited to about 3.0 μm to keep the overall size of the cell small, maintain its flexibility, and ensure that the cell does not become too wide to harvest the available carriers before recombination occurs.

Typically, an *n*-type cadmium sulfide (CdS) thin film is used as a fourth buffer layer. This buffer layer serves as the *n* portion of the *p-n* junction and typically has a thickness of 0.05-0.1 μm [17]. CdS is a good choice for this buffer layer because it has a bandgap of 2.4 eV, which allows a majority of photons to pass through to the Cu(InGa)Se2 absorber layer

[18]. Only photons with a wavelength shorter than 500.0 nm can be absorbed by the CdS layer. While most Cu(InGa)Se_2 solar cells produced use the CdS, it is undesirable due to the fact that it falls into the category of heavy metals and creates concerns for both the environment and anyone who comes into contact with it. Furthermore, the use of a CdS buffer layer requires a thin intrinsic ZnO layer to be deposited between the buffer layer and the transparent conducting oxide layer which adds an additional step to the manufacturing process.

The top layer is a ZnO window layer. It consists of a very thin intrinsic ZnO layer topped with an aluminum (Al) doped ZnO transparent conducting oxide layer. This layer serves to allow for photons to pass through while simultaneously allowing for the conduction of current generated by the cell [17].

The top contact is placed on top of the window layer and is typically made of a grid of Al. This is necessary to allow for the collection of carriers generated within the solar cell.

II.2.2. Developments in Cu(InGa)Se_2design:

Several studies have been published aimed at comparing buffer layers to determine if a viable alternative to CdS exists. The most promising is the use of an *n*-type ZnO buffer layer in place of the traditional CdS. ZnO has a bandgap of 2.8 eV, which increases the wavelength spectrum that passes through the buffer layer into the absorber layer [18]. Despite the promise of ZnO buffer layers, many studies demonstrated that using ZnO in place of CdS results in a cell with a 3–5% lower efficiency [17]. Regardless, some companies and researchers continued exploring the use of ZnO as an alternative to CdS. Record setting cells with efficiencies nearing 21% were fabricated using the ZnO buffer layer, proving that ZnO remains a viable replacement for CdS as the buffer layer in a CIGS cell [22].

Another advancement in the design of Cu(InGa)Se_2 cells is the inclusion of graded Ga concentration within the absorber layer in order to increase the overall efficiency of the solar cell. The first method is known as back grading, where the concentration of Ga is increased moving towards the back contact. The second method is known as front grading, where the Ga concentration is decreased moving towards the back contact. The third is essentially a blend of the first two concepts, in which higher Ga concentration at both the top and bottom contacts is achieved with a minimum Ga concentration in the middle of the absorber layer [23].

II.3.Trap density in CIGS alloys:

One of the primary concerns in the design of Cu(InGa) Se_2 solar cells is the determination of the Ga concentration to be used. Given the tunable bandgap that Cu(InGa)Se_2 possesses, it was initially thought that a higher Ga concentration, which leads to a higher bandgap, would result in a cell with a higher efficiency. Through experimentation, it was found that this was not the case; an ideal Ga concentration of around 0.3 mole fraction has been found to result in the highest efficiency cells [17]. This phenomenon required investigation as to why the efficiency did not follow the expected increase predicted by theory.

Recently, a study published measured the trap density within Cu(InGa)Se_2. It was found that trap density is a function of Ga concentration [24]. The relationship between trap density and bandgap, which is directly proportional to mole fraction, is illustrated in Figure 10. The result is that the increases in efficiency that are expected from a higher Ga concentration are offset by the higher trap density associated with that higher Ga concentration, supporting the idea that cells with Ga mole fractions around 0.3 achieve the highest efficiencies [24]. Furthermore, this plot includes data from an analysis of devices produced by both the single-stage process as well as the three-stage process. The conclusion is that the three-step process results in a better overall structure with fewer defects [24].
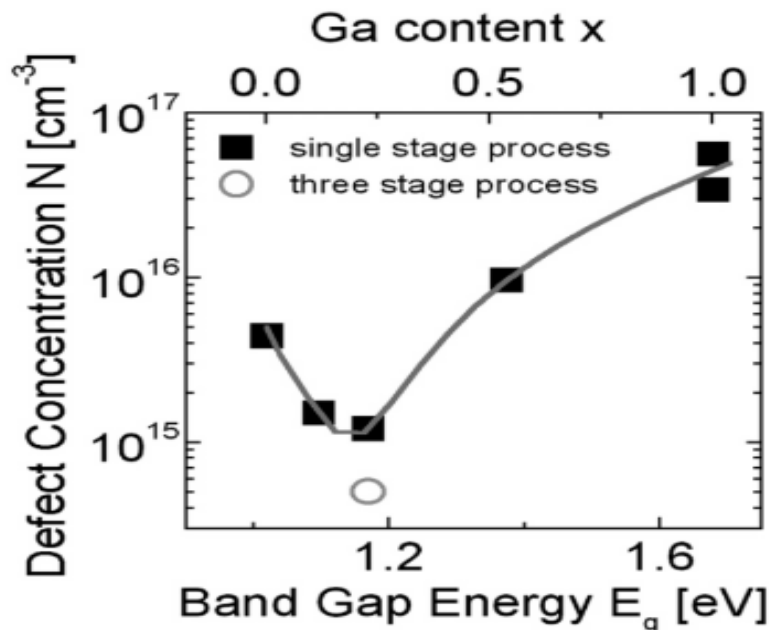
Figure II.3: Plot of defect concentration versus Ga composition [24].

The study from which Figure II.3 originated was limited to a single data point for the three-stage process, which does not provide a sufficient basis for this trap density to be

used. Further studies of the density of traps have resulted in a wide range of reported values for the trap density in Cu(InGa)Se_2 produced using the three-stage process. Most trap densities are reported with a magnitude of 10^{14}; a more realistic profile was created based on these results as illustrated (Figure II.4) [25]. The minimum trap density reported is 1.2×10^{14} for a mole fraction of 0.24. Results have been reported for trap densities measured an order of magnitude or more [25], [26] less than the results (Figure II.3). The profile of average reported trap densities for Cu(InGa)Se_2 produced using the three-stage process is illustrated (Figure II.4).
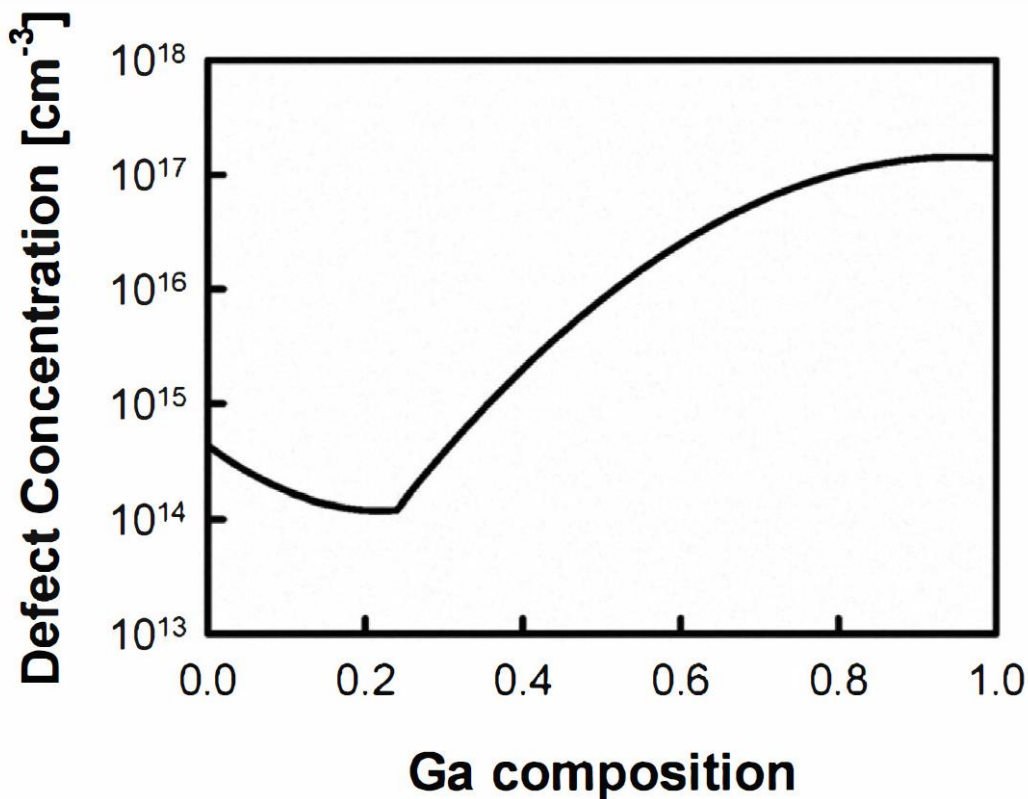
Figure II.4: Average defect concentration as a function of Gacomposition[25].

II.4.Device Physics:

When the p-type buffer layer and n-type CIGS absorber layer come into contact, a p-n junction is formed. The process is out lined (figure II.5).The p-type material, although Electrically neutral is doped to have an excess of holes (acceptor states). The n-type material, also electrically neutral, is doped to have an excess of electrons (donor states).When the two materials make contact, a junction forms.
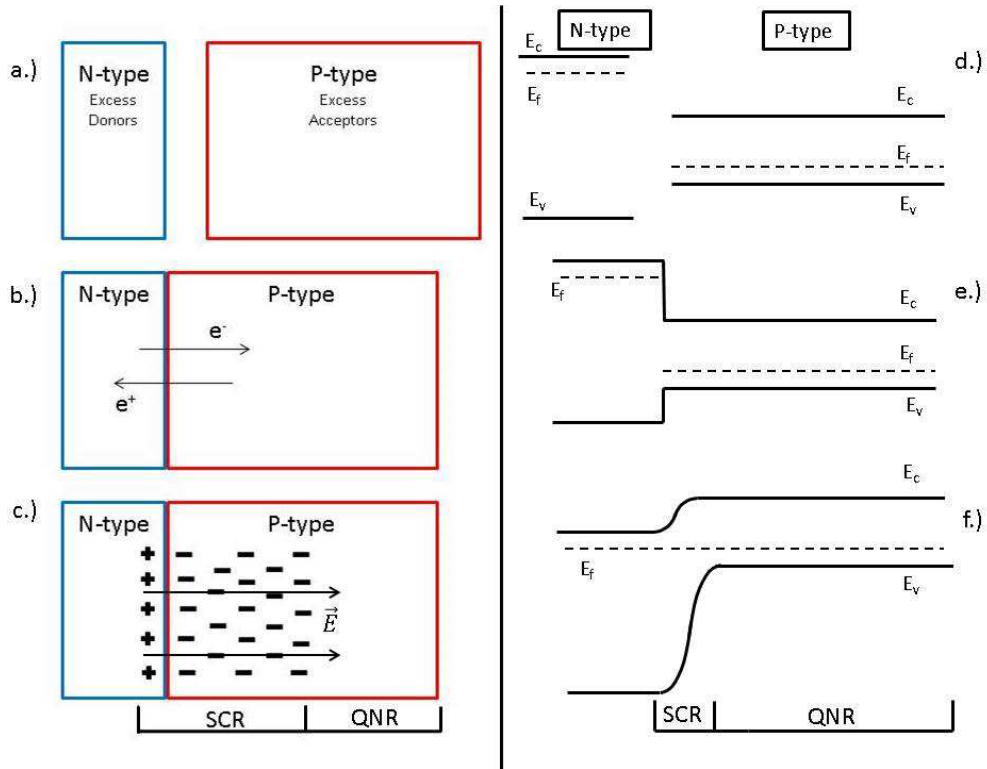
Figure II.5: a-c: p-n junction and formation of the space-charge region, d-f: corresponding band diagrams

Since there is a concentration gradient of charge carriers between the two materials, electrons from the n-type material migrate to the p-type material and combine with holes, leaving behind a positively charged ion. Holes from the p-type material migrate to the n-type material to combine with electrons, leaving behind negatively charged ions (Figure II.5b). This is known as diffusion current. The accumulation of charged ions in each material creates an electric field which is referred to as the "built-in field". The region the built-in field extends over is called the space-charge region (SCR). The SCR is stabilized when the drift current caused by the built-in field equals the diffusion current.

The width of the SCR in the p-type material Wp and in the n-type material Wn is based on the depletion approximation, which assumes the depleted charge has a box profile and is dependent on the doping densities, N_A for acceptor impurities, and N_D for donor impurities [27].

$$N_A W_P = N_D W_A \tag{III.3}$$

The band diagram shown (figure II.5f) is a useful way of looking at a p-n junction. A charge carrier can either be bound to an atom (in the valence band) or able to move freely

throughout the material (in the conduction band). The Fermi-Dirac distribution describes the occupancy of states in a material, and the Fermi level is the energy of average occupancy, essentially the average electron energy. In an n-type semiconductor, (which has a larger concentration of free electrons) the Fermi level lies closer to the conduction band, while in a p-type semiconductor (low concentration of free electrons) the Fermi level lies closer to the valence band (figure II.5d). To satisfy the zero current condition associated with thermal equilibrium, the Fermi levelthroughout the sample must be constant. When put in contact, the Fermi levels of the two materials line-up, causing a shift in band alignment (figure II.5e-f). The SCR can be looked at as a shift in the energy bands at the junction. Electron hole pairs generated in the SCR are swept across the band and collected at the electrical contacts. This is called drift current.

The part of the absorber that is not part of the built-in field is called the quasi neutral region (QNR). Electron-hole pairs generated in this region are not immediately swept across the junction. Their movement is dependent on carrier lifetime and diffusion length, also their direction of movement is random. Due to the absorption capability of CIGS the width of a cell may need to be large enough to allow for a depletion region capable of collecting deeper penetrating long wavelength photons and to avoid recombination losses that may result from generation near the back contact junction. An example CIGS band diagramisdisplayed(figure II.6).
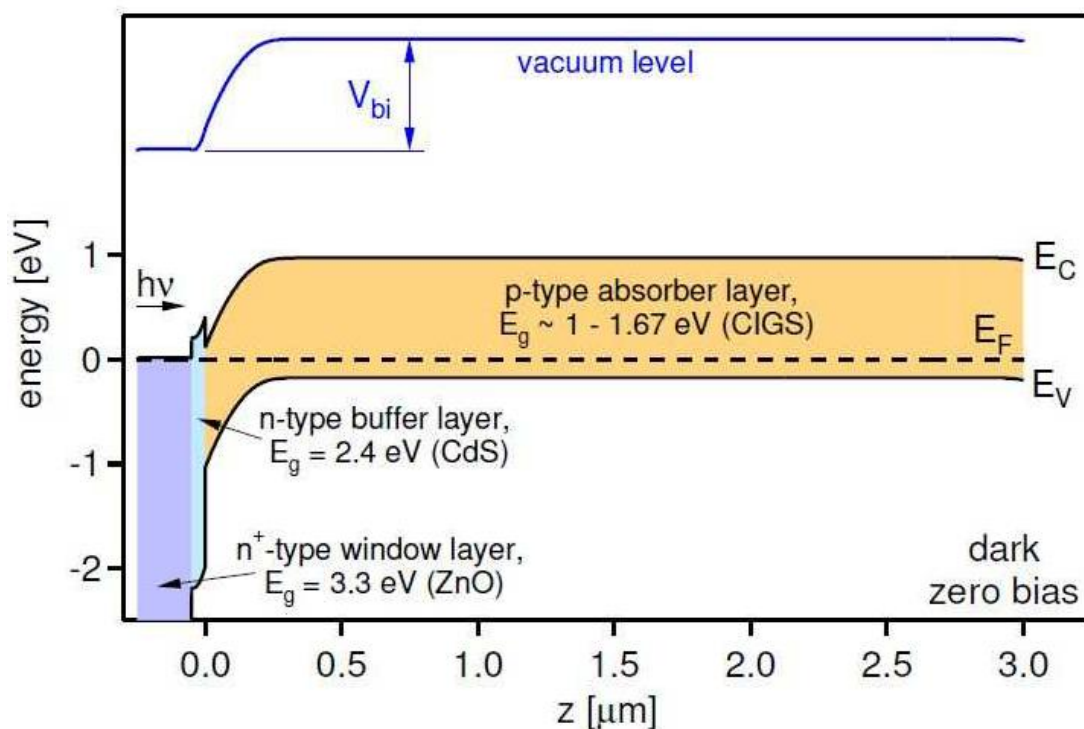
Figure II.6:CIGS band diagram [28].

II.5.conclution:

In this chapter, we have presented an overview on the CIGS solar cells, where we presented the composition of the CIGS –based solar cell, and the role of each of the layers that compose it. We also talked about developments in CIGS solar cell design; the CIGS alloys trap density and finally the physics of the CIGS solar cell device.

Chapter III:

CIGS-based solar cell simulation

III.1.Introduction:

Modeling using software provides a fast, consistent, and relatively inexpensive way to design solar cells. Modeling and simulation allowed for thousands of combinations to be investigated before the fabrication of actual examples. The use of Silvaco-Atlas simulation software to model a CIGS based-solar cell, and evaluate its performance for different variations of the solar cell parameters, such as the ambient temperature, is the focus of this thesis.

In this chapter, we will talk about Silvaco-Atlas simulation environment and the device basic construction layout.

III.2.Silvaco simulation environment:

Simulation of a photovoltaic (PV) cell in Silvaco-Atlas is made through a text input deck called DeckBuild, a run-time environment in which many different parameters of cell structure and composition must be defined.

The structure definition comprises a cornerstone for the simulation since it not only bears the physical dimensions and thicknesses of the different layers constituting the cell but also builds a mesh for the cell through its fine division. Its significance is that at the grid points, called nodes, a set of differential equations are solved with a view to simulating the transport of the cell's carriers and enabling a study of the behavior of the cell.

The composition definition is also important since Silvaco-Atlas is a physically-based device simulator. Once the physical structures are specified, composition and bias conditions statements lead Silvaco-Atlasto make predictions of the electrical characteristics of the cell.

The buildup consists of a well-defined mesh on which the cell is constructed. The simulation's resolution is determined by the density of the mesh's numerous triangles and designates the time needed for program iterations and the accuracy of cell representation. This triangulate mesh is then divided into regions, and different materials are assigned in each of those regions. Then, the electrodes to obtain the electrical characteristics for the device or for any region required are assigned. Next, every defined material must be

associated with a doping, and, as much as possible, material properties must be declared for the most accurate simulation. The next step for the user is to choose among different models, finding that which is most the suitable for evaluating the structure, and achieving a better outline for the specific cell simulation. A specification of a light beam illuminates the cell as in real conditions, simulating different regions of the solar spectrum, depending on the beam chosen. Also, the selection of a method, among the different offered by the Silvaco-Atlas library, is needed for solving the differential equations through which the cell's operating characteristics arise. These characteristics from the simulation can be saved in a log file and used to create plots using TONYPLOT, the interactive graphics and analysis package are included in the program. The preceding analysis of cell buildup is illustrated (figure III.1).

Figure III.1: Command group and statements layout for a Silvaco-Atlas file. [29]

III.3. Device basic construction layout:

The first line to be read by the program when running Silvaco-Atlas using DeckBuild is the GO ATLAS command. After that, the statements structure should be followed in the sequence depicted(Figure III.1). AnSilvaco-Atlas comprisedof a keyword and a set of parameters, which are not case sensitive, in the following format:

<STATEMENT><PARAMETER>=<VALUE>.

An example of theSilvaco-Atlas syntax for defining the material properties is given by:

MATERIAL MATERIAL=CdS EG300=2.4 PERMITTIVITY=10

AFFINITY=3.75 MUN=10 MUP=1 NC300=2.2e18 NV300=1.8e19.

The statement is 'MATERIAL' and is used to set basic material parameters related to band structure and parameters for certain mobility, recombination, or carrier statistics models. The parameters are MATERIAL, EG300 PERMITIVITY, AFFINITY, MUN, MUP, NC, NV. There are four groups of parameters: real, integer, character, and logical. The 'MATERIAL' parameter is of type 'character', which is any character string. All the other parameters used in this example are of type 'real', meaning they must be real, not imaginary, values. Integer parameters can take on integer values, while logical parameters imply a true or false condition.

An interesting observation can be made on the use of the backslash '\' at the end of a line of code. The program is informed that the following line of code should be considered a continuation of the line of code in which this symbol has been introduced [29].

III.3.1.Mesh:

The grid consists of horizontal and vertical lines with a user-defined distance between them. It bounds the physical area of the cell by creating a number of triangles in which the simulation will take place. Mesh specification also involves a tradeoff between accuracy and numerical efficiency. A fine defined mesh will lead to more accurate results, and on the other hand, a coarse mesh that minimizes the total number of grid points will lead to a larger numerical efficiency.

The mesh is created with the following statements:

MESH SPACE.MULT=<VALUE>;

X.MESH LOCATION=<VALUE> SPACING=<VALUE>;

Y.MESH LOCATION=<VALUE> SPACING=<VALUE>.

The default value for the mesh scaling factor is one but can be changed at will. Values smaller than the default create a finer grid, containing enough points to be accurate. In contrast, larger values create a crude grid, especially in material boundaries and junctions, leading to less accurate results. Vertical and horizontal mesh division, in microns, is specified with X.MESH and Y.MESH commands and their associated spacing.

An example of both fine and coarse meshes designed in Silvaco-Atlas is depicted (Figure III.2).
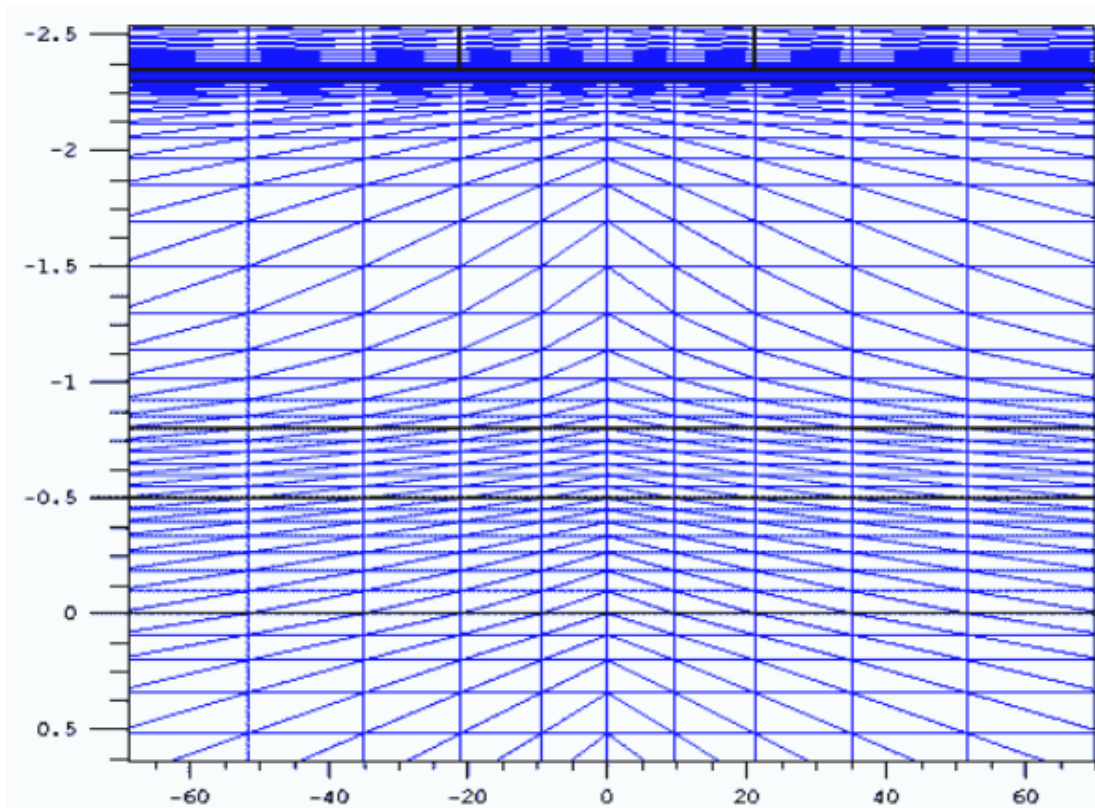
Figure III.2: Typical mesh in Silvaco-Atlas

III.3.2.Regions:

In defining a region, all locations of the mesh are divided into numbered areas, where each is associated with a specific material from theSilvaco-Atlas library. Regions are created with the following statements:

REGION number=<integer><material type><position>.

The number assigned to each region is representative of this area, which now can be called and stated by this number. Determining the position of each region attests that the region's limits will not exceed the limits of the grid, which are the physical bounds of the cell.

III.3.3.Electrodes:

Electrodes specify the locations and names of electrodes in the previously defined mesh. This location can be any specific region, and for the purposes of this thesis, a pair of cathode, and anode electrodes was assigned in the two individual cells that form the tandem CIGS cell. The format to define the electrodes is:

ELECTRODE NAME = <electrode name><position>.

BOTTOM and TOP statements specify that the electrode is positioned along the bottom or the top of the device, respectively. Otherwise, minimum and maximum position boundaries must be specified, using the X.MIN, X.MAX, Y.MIN, Y.MAX statements.

III.3.4.Doping:

DOPING specifies doping profiles in the device structure, either analytically or from an input file. The DOPING statement is:

DOPING <distribution type><dopant type><position parameters>.

Uniform, Gaussian or non-standard (user defined from a custom file) distributions can be used to generate the doping profile. The type and concentration of doping must be defined next as well as the region to be doped.

III.3.5.Material:

The previously defined and doped region must be associated with specific materials. These materials, their properties, and physical parameters can be selected from the Silvaco-Atlas database, among a number of elements, compounds, and alloys. The user specifies the material and its properties using the general statement form:

MATERIAL <localization><material definition>.

A specific example used in this thesis is:

MATERIAL MATERIAL=CdS EG300=2.4PERMITTIVITY=10 \

AFFINITY=3.75 MUN=10 MUP=1 NC300=2.2e18 NV300=1.8e19.

In this example, the material used is the CdS with band gap equal to 2.4 eV, dielectric permittivity equal to 10 F/m, and electron affinity equal to 3.75 eV. More properties include low-field electron and hole mobility, in cm^2/Vs units, equal to ten and one, respectively. Also, the conduction and valance band densities at 300 K are equal to $2.2 \cdot 10^{18} cm^{-3}$ and $1.8 \cdot 10^{19} cm^{-3}$, respectively.

These material properties and physical parameters are defined for every region consisting of the specific material. The user can change the material properties only in a region by replacing the second MATERIAL from the above example with a REGION statement describing this specific region.

III.3.6.Models:

Once we define the mesh, geometry, and doping profiles, we can modify the characteristics of electrodes, change the default material parameters, and choose which physical models Silvaco-Atlas will use during the device simulation. The physical models are grouped into five classes: mobility, recombination, carrier statistics, impact ionization, and tunneling, and details for each model are contained in the Silvaco-Atlas user manual [29]. The general MODELS statement is:

MODELS <model name>.

Physical models can be enabled on a material-by-material basis. This is useful for hetero junction device simulation and other simulations where multiple semiconductor regions are defined and may have different characteristics.

III.3.7.Solution Method:

The numerical methods to be used for solving the equations and parameters associated with these algorithms are determined by the METHOD statement. Several numerical methods are contained in theSilvaco-Atlas library, but there are three main types. The GUMMEL method is used for weakly coupled system equations, with only linear convergence. The NEWTON method is used for strongly coupled system equations, with quadratic convergence, requiringSilvaco-Atlas to spend more time solving for quantities which are essentially constant or weakly coupled. Toobtain and ensure convergence, a more accurate approximation is needed from the system. Finally, the BLOCK method

provides faster simulations when the NEWTON method is unable to provide a reliable solution [29].

III.3.8.Light Beam:

An optical beam is modeled as a collimated source using the BEAM statement of the form:

BEAM <parameters>.

The origin of the beam is defined by parameters X.ORIGIN and Y.ORIGIN, the ANGLE parameter specifies the direction of propagation of the beam relative to the x-axis, while ANGLE=90 describes a vertical illumination from the top of the device. The beam is automatically split into a series of rays so that the sum of the rays covers the entire width of the illumination window. When the beam is split, Silvaco-Atlas automatically resolves discontinuities along the region boundaries of the device. Rays are also split at interfaces between regions into a transmitted ray and a reflected ray [29].

For the purposes of this thesis, the source is the sun, and the AM1.5 spectrum is used to simulate the energy received by a solar cell in a terrestrial application.

III.3.9.Solution Specification:

Silvaco-Atlas can calculate DC, AC small signal, and transient solutions. Obtaining solutions is similar to setting up parametric test equipment for device tests. The user usually defines the voltages on each electrode in the device. Silvaco-Atlas then calculates the current through each electrode and the internal quantities, such as carrier concentrations and electric fields throughout the device.

In all simulations, the device starts with zero bias on all electrodes. Solutions are obtained by stepping the biases on electrodes from this initial equilibrium condition. To obtain convergence for the equations used, the user should supply a good initial guess for the variables to be evaluated at each bias point. The Silvaco-Atlas solver uses this initial guess and iterates to a converged solution. Solution specification can be divided up into four parts: LOG, SOLVE, LOAD, and SAVE.

Log files store the terminal characteristics calculated bySilvaco-Atlas. These are thecurrents and voltages for each electrode in DC simulations. For example, the statement:

LOG OUTF=<FILENAME>

is used to open a log file, and terminal characteristics from all SOLVE statements after the LOG statement are then saved to this file. Log files contain only the terminal characteristics and are typically viewed in TONYPLOT.

The SOLVE statement follows a LOG statement and instructs Silvaco-Atlas to perform a solution for one or more specified bias points.

The LOAD and SAVE statements are used together to help create better initial guesses for bias points. The SAVE statement saves simulation results into files for visualization or for future use as an initial guess, and after that the LOAD statement loads a solution file whenever required to assist in the solution.

III.3.10.Data Extraction and Plotting:

Extracting the data and plotting it is the final section of the input deck. The EXTRACT statement is provided within the DeckBuild environment. It has a flexible syntax that allows the user to extract device parameters and construct specific EXTRACT routines. By default, EXTRACT statements work on the currently open log file, are generally case sensitive, and operate on the previous solved curve or structure file. All graphics inSilvaco-Atlas are performed by saving a file and loading the file into TONYPLOT. The log files produced by Silvaco-Atlas and the current-voltage cell characteristic can be plotted and observed in TONYPLOT.

III.4.Conclusion:

In this chapter, we have presented the function of Silvaco-Atlas, as simulation tool to evaluate, and predict, the performance of a CIGS –based solar cell. Also was presented a quick look at the operating principle, and means to input different parameters for the best possible simulation of the solar cell. Using the simulation capabilities of Silvaco-Atlas software, we will builta CIGS-based solar cell to study the ambient temperature effect.

Chapter IV:

Temperature effect on the performance of Cu(In,Ga)Se$_2$ (CIGS)-based solar cell

Chapter IV: temperature effect on the performance of Cu(In,Ga)Se$_2$ (CIGS)-based solar cell

IV.1. Introduction:

In this chapter, we present the study resultsof the performance of a Cu(In,Ga)Se$_2$ (CIGS)–basedsolar cell, achieved by the SILVACO-ATLAS numerical simulation software,which allows the computation of all the internal parameters of the solar cell such as the distribution of the band diagram, electron and holesconcentrations, the recombination rate, as well as the external parameterssuch as the currentdensity-voltage ($J - V$) characteristic,from which the outputphotovoltaic parameters,characterizing the solarcell performance, can be extracted, namely the short circuit current density J_{sc}, the open circuit voltage V_{oc}, the fill factor FF,the maximum power P_{max} provided by the cell and the photovoltaic conversionefficiency η of the cell. The aim of this work is to study the effect of ambient temperature on the performance of the solar cell exposed to theAM1.5 standard spectrum in terms of the effect on both internal and external parameters.The considered temperature range is [230°K-350°K] equivalent to [(-43°C)-(77°C)]. The solar cell may be exposed to the low temperature,for example, through the climatic conditions of cold regions.The cellmay be exposed tohigh temperature for example, when it is continuously exposed to solar radiation in hot regions.

IV.2. Description of the studied CIGS-based solar cell:

The solar cell structure, under consideration,in this study is mainly of mono crystalline CIGS material and is shown in figure IV.1 from the SILVACO-ATLAS softwarerepresentation. The cell is composed of the following layers: n-type doped ZnO layer, n-type dopedCds layer, p-type doped CIGS layer and metallic conduction electrodes that allow the conduction of the generated electrical currenttothe external circuit.The cathode is on the top of the cell and the anode ison the bottom of the cell because the cell junction is nnp-type.

. **CIGS**: is a layer of 1.5μm to 3μm thickness deposited over the substrate. It is a p-type semiconductor called an absorbent, where photons are absorbed and create pairs of electron-hole.

CdS: a thin n-type cadmium sulphide film used as a fourth dielectric layer. It has a band gap of 2.4 eV, which allows the majority of photons to pass into the Cu(In,Ga)Se_2absorbent layer.

ZnO: it is a n-type window layer consisting of a very thin layer topped by a layer of zinc oxide doped with aluminum symbolized by (ZnO: Al), this layer works to allow the photons to pass through while allowing at the same time to conduct the current generated by the cell.
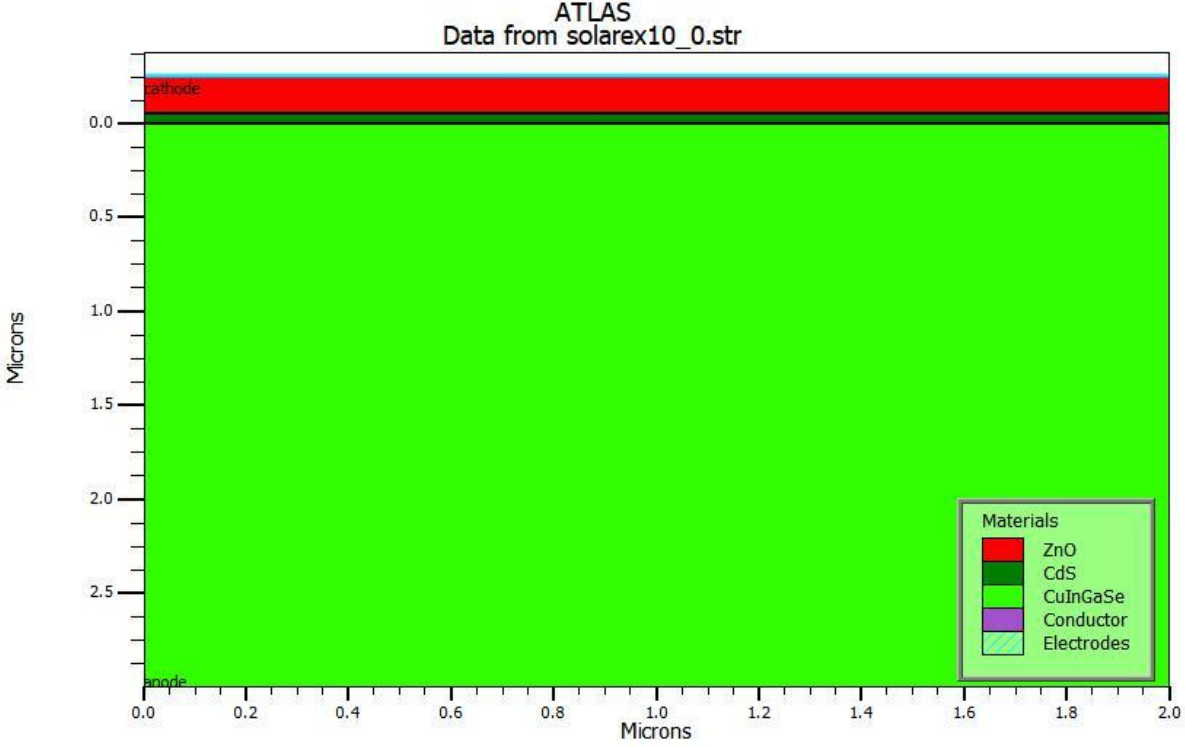
Figure IV.1: Structure of the studied CIGS-based solar cell.

Table IV.1: Input parameters of the CIGS-basedsolar cell simulated by Silvaco-Atlas

Parameters		Value
Cellthickness, d (µm)		3.25
Cell wide, x_{tot} (µm)		2
Thickness (µm)	ZnOregion	0.2
	CdSregion	0.05
	CIGSregion	3
Doping (n-type) (cm^{-3})	ZnOregion	10^{18}
	CdSregion	1.1×10^{18}
Doping (p-type) of CIGSregion (cm^{-3})		2×10^{16}
Energy gap, E_g (eV)	ZnOregion	3.3
	CdSregion	2.4
	CIGSregion	1.15
Permittivity, ε_r	ZnO region	9
	CdS region	10
	CIGS region	13.6
	ZnO region	4.7

Chapter IV: temperature effect on the performance of Cu(In,Ga)Se$_2$ (CIGS)-based solar cell

Affinity, χ (eV)	CdS region	4.5
	CIGS region	4.8
Electron mobility, μ_n $(cm^2V^{-1}s^{-1})$		100
Hole mobility, μ_p $(cm^2V^{-1}s^{-1})$		25
Effective densityat E_C, N_C (cm^{-3})		2.2×10^{18}
Effective density atE_V, N_V (cm^{-3})		1.8×10^{19}
Anode work function(eV)		5.75
Cathode work function(eV)		4.7

Table IV.2: Defect parameters used in the simulation

Defect type	ZnOregion	Donors
	CdSregion	Acceptors
	CIGSregion	Donneurs
Defectdensity	ZnOregion	$10^{17}cm^{-3}$
	CdSregion	$10^{18}cm^{-3}$
	CIGSregion	$10^{14}cm^{-3}$
Defect distribution	ZnOregion	Gaussien
	CdSregion	Gaussien
	CIGSregion	Gaussien
Electron capture section	ZnOregion	$10^{-12}cm^2$
	CdSregion	$10^{-17}cm^2$
	CIGSregion	$5 \times 10^{-13}cm^2$
Hole capture section	ZnOregion	$10^{-15}cm^2$
	CdSregion	$10^{-12}cm^2$
	CIGSregion	$10^{-15}cm^2$
Energylevel position	ZnOregion	1.65 eV
	CdSregion	1.2 eV
	CIGSregion	0.575 eV

Given that the studied solar cell operates under the conditions ofthe AM1.5standard solar spectrum, the optical constants (n, k) for each of the regions ZnO, Cds and CIGS are represented by the extinction coefficient k(or the absorption coefficient$\alpha = \frac{4nk}{\lambda}$) and the optical index of refraction$n$ are experimental data that Silvacokeeps in its database and can be plotted from it as shown in figure IV.2.
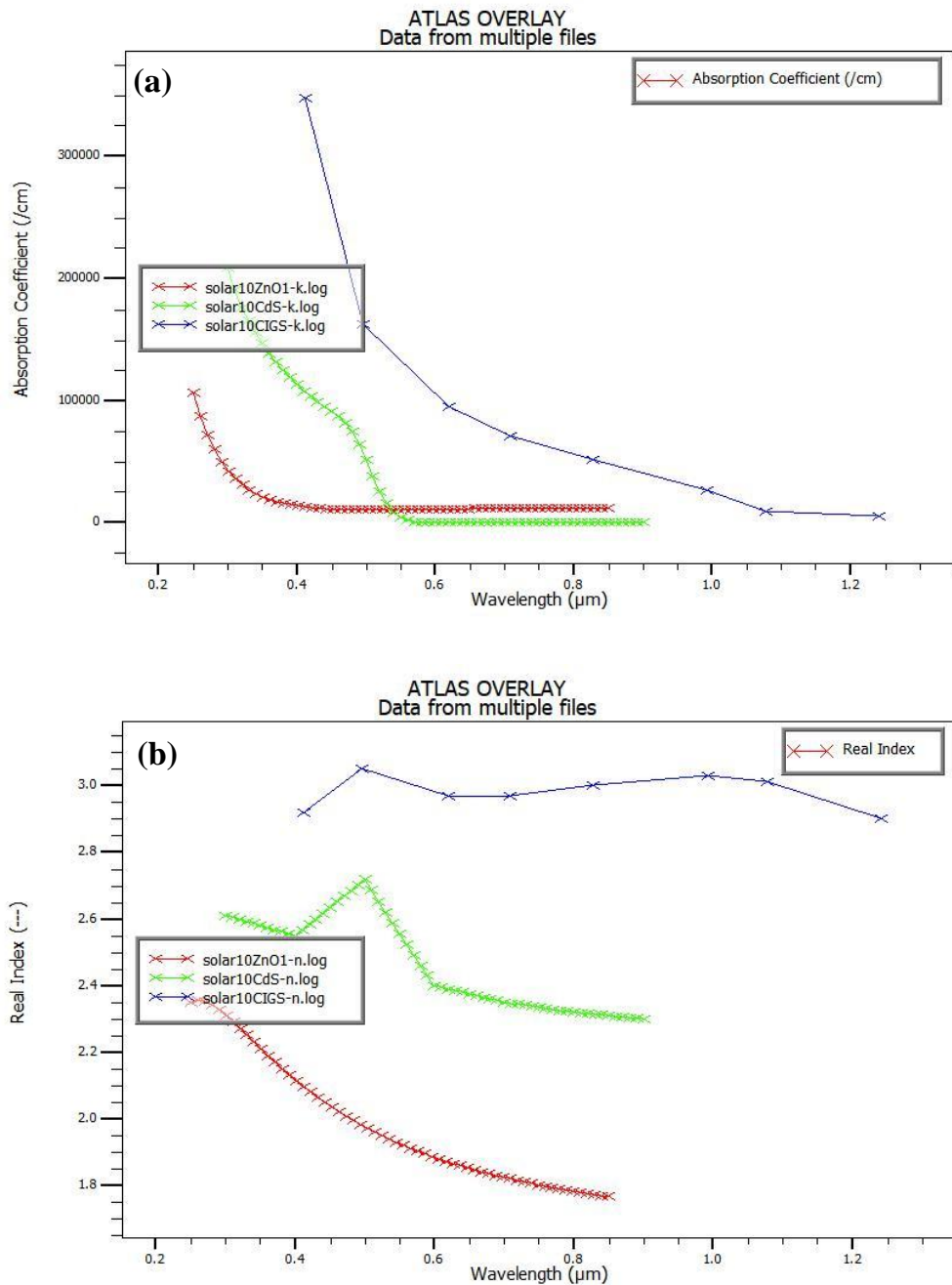
Figure IV.2 : Optical constantsof ZnO, CdS and CIGS regions of the CIGS-based solar cell : (a) absorption coefficient (α), (b) optical index of refraction (n), from SILVACO data base.

To study the considered solar cell by numerical simulation, the Silvaco-Atlas software divides the studied cell spatially (spatial mesh) according to the finite elements method. This means that the studied device is dividedinto infinitesimal triangle forms, and this is

shown in two dimensions (2D) in figure IV.3. This latter includes as well as a miniature image (zoom) that enlarges the upper part of the cell to clarify the space division in it.

The spatial discretisation allows that transport equations (Poisson and the charge carrier continuity equations) can be solved numerically, and consequently, the calculation of all internal physical quantities such as the concentrations of charge carriers and the potential or the electric field distribution, the electron and holecurrent densities, the band diagram, the recombination rate, etc…. in all nodes formed through the spatial division, and then, to calculate the external quantities such as the total electric current density and the currentdensity -voltage $(J - V)$ characteristic.
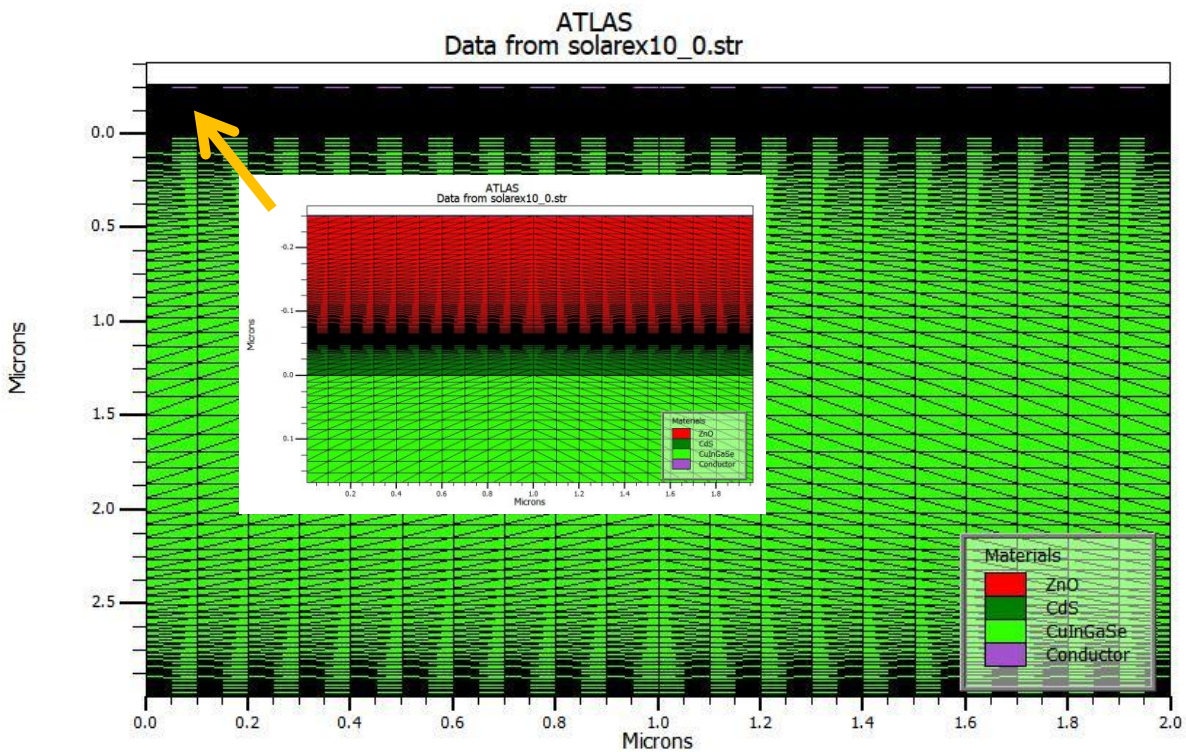
Figure IV.3: Two dimensional (2D) meshof the CIGS-based solar cell.

The more accurate the spatial division is, the more accurate the results are also.

This solar cell device is based onCIGS material.Through theSilvaco-Atlas software numerical simulation,which divides the device spatially as shown on figure IV.3, and after entering allofthe input data shown in the tables IV.1 and IV.2, the Silvaco–Atlas softwaresolves the transport equation by numerical methods, and then calculates all of the internal and external physical parameters of the cell. So studying the cell under the

temperature change effect in the range[230°K-350°K], means the calculation of theinternal physical quantities such as distributions of electron and hols concentrations, banddiagram, recombination rate ...etc under the temperature changeeffect, and then the deductionof the external quantities under the same effect of temperature change, i.e., calculating the currentdensity-voltage $(J - V)$ characteristic for different temperature, andextractingthe values of the photovoltaic parameters characterising the cell performance, represented by the short circuit current density J_{sc}, the circuit voltage the open V_{oc}, the fill factor FF, the maximum powerprovided by the cell P_{max} , and the photovoltaic conversion efficiency η of the cell, under different temperatures.

IV.3. Results and discussion:

The study results are presented in this section. Firstare presentedthe internal parametersdistributions of the solar cell such as the distribution of the energy band diagram (or the band gap profile), the distribution of free electron and hole concentrations(free carrier densities), and the recombination rate distribution.In in the second part,we present the the current density-voltage $(J - V)$ characteristic and the photovoltaic parameters. All internal and external parameters are studiedunder the temperature change effect in the range$[230°K - 350°K]$.

In order to plot the internal parameterdistribution, figureIV.4 shows this for the example of theCIGS solar cell band diagram at thermal equilibrium and ambient temperature of 300°K.

We draw a vertical line, the so-called(cut line) parallel to the (Oy) axis that cuts the axis (Ox) in a specific position, for the example of figure IV.4, it cuts the axis (Ox) approximately at x= 1μm.This line will also intersect with lines of the device spatial discretisationin several points, from the top of the device to the bottom of it.At these points Silvaco computes the values of the internal quantities such as the values ofE_C, E_V, quasi-Fermilevel of the electrons E_{fn}, and quasi-Fermi level of the holesE_{fp}. These quantities will from the energyband diagram of the solar cell that can be plottedin thermal equilibrium, as shown by both figures IV.4 and IV.5.In thermal equilibrium,the quasi-Fermi level of electrons coincides withthe hole quasi-Fermi level, and together are formingthe thermal equilibrium Fermi-levelE_f which is horizontal (or flat).
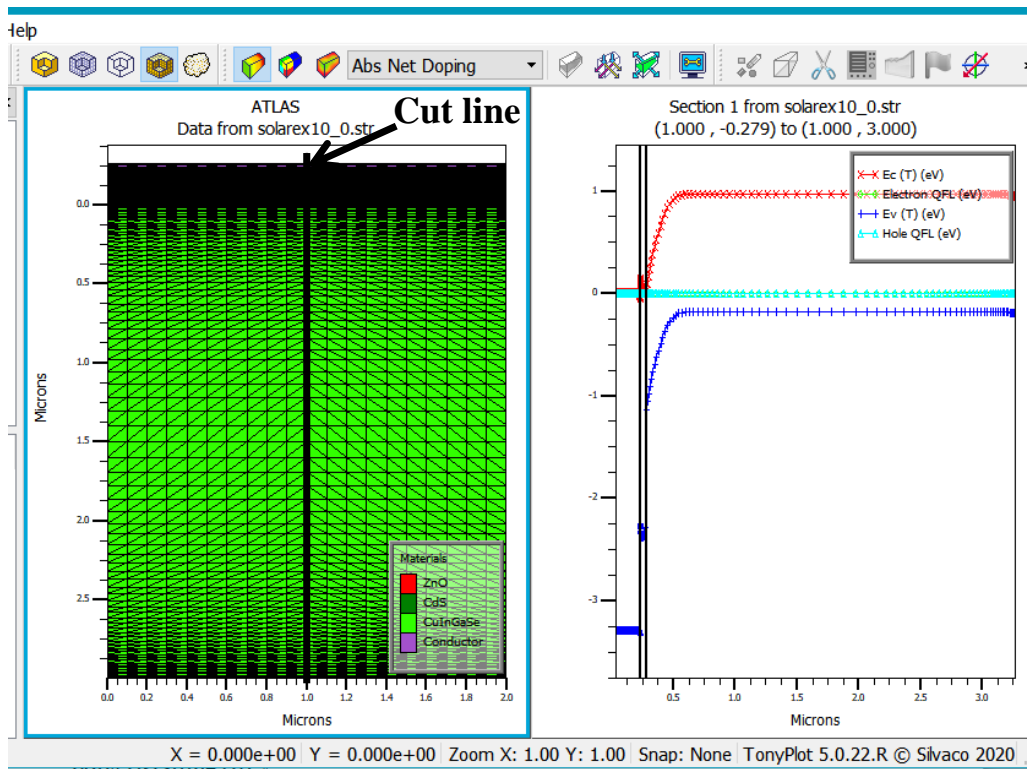
Figure IV.4: Plotting of the band diagram in SILVACO-ATLAS for the CIGS-based solar cell at thermal equilibrium and T=300°K.
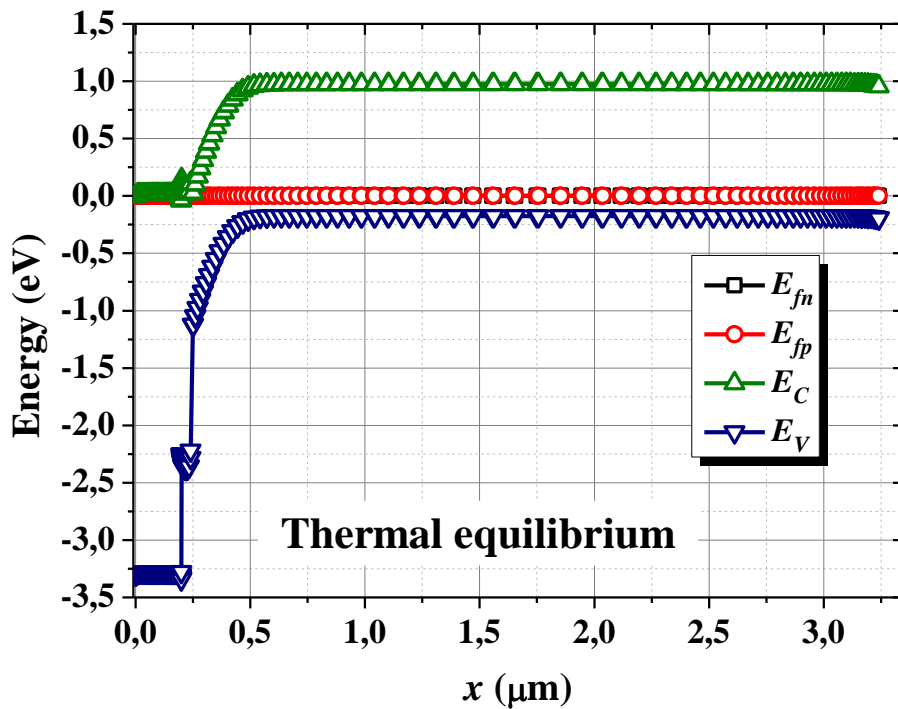
Figure IV.5: Band diagram of the CIGS-based solar cell at thermal equilibrium and T=300°K.

In the same way, the energy banddiagram can be plotted in short-circuit conditions asshown in figure IV.6 for T $= 300°K$.
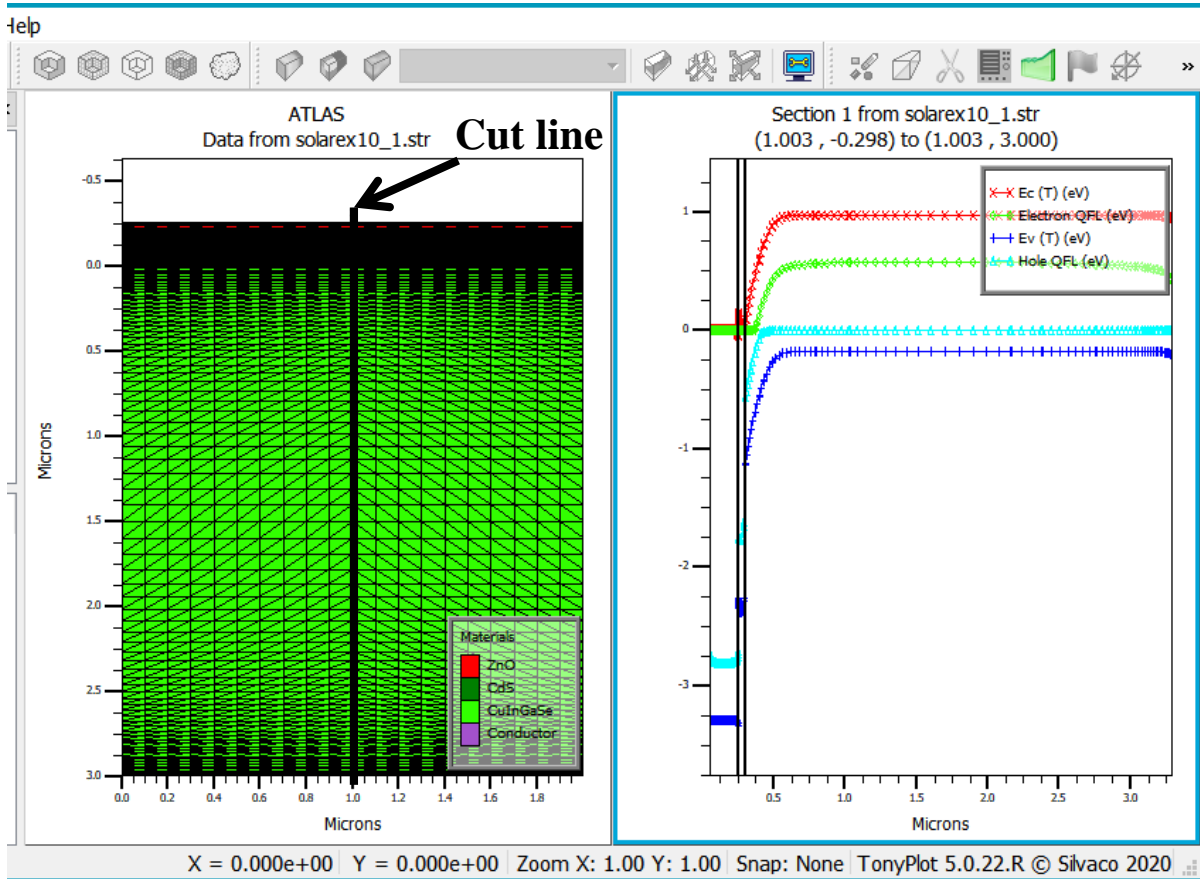
Figure IV.6: Plotting of the band diagram in SILVACO-ATLAS for the CIGS-based solar cell at short-circuit condition and T=300°K.

In that case, the current reaches its largest value which is the short circuit currentdensity J_{sc}. However, the voltagedifferencebetween the two solar cell contacts is null. Here, the quasi-Fermilevel E_{fn} of the electrons in the p-type CIGS region rises from the quasi-Fermi level of holesthe E_{fp} , expressing a significant increase,bylight absorption,of the electrons that are minority carriers in the p-type CIGS base region, as shown in figure IV.6. The hole quasi-Fermi level E_{fp} in the CIGS region remains horizontal in the same position as it was at thermal equilibrium because the holes are majoritycarriersin the p-typeCIGS region, and the hole concentration is of the same order as the p-type dopinggiven in table IV.1($2 \times 10^{16} cm^{-3}$). Then, thehole concentration increase, by the light absorption, is not significant compared to the concentration of the dominant p-type doping. So the total hole concentrationremains approximately equal to the

thermal equilibrium concentration, and the holequasi- Fermi levelE_{fp},in the CIGS region, remains horizontal in the same position as it was at thermal equilibrium.

By applying the same cut line method, it is possible,in addition to the band diagram,to plot the distribution of all the internal parameters calculated by Silvaco-Atlas, such as the distribution of the charge carrier concentrations ofelectrons (n) and holes (p),recombination rate, potentialdistribution, current component of electrons and holes...etc.

Figure IV.7 shows, for example, the distribution of the charge carrier concentrations of electrons (n) and holes (p) in short circuit conditions at ambient temperature T = 300°K. Figure IV.8 shows the electrical potential distribution inside the cell always under short circuit conditions at ambient temperature T = 300°K.
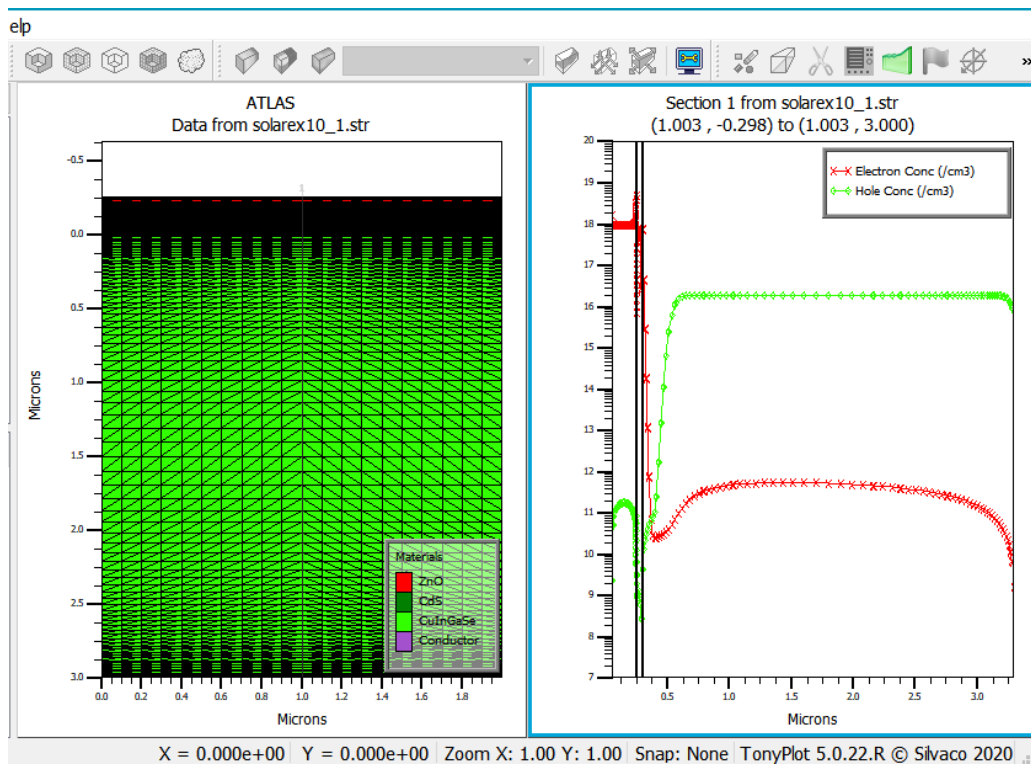
Figure IV.7: Free carrier density profile inside the CIGS-based solar cell at short-circuit condition and T=300°K.
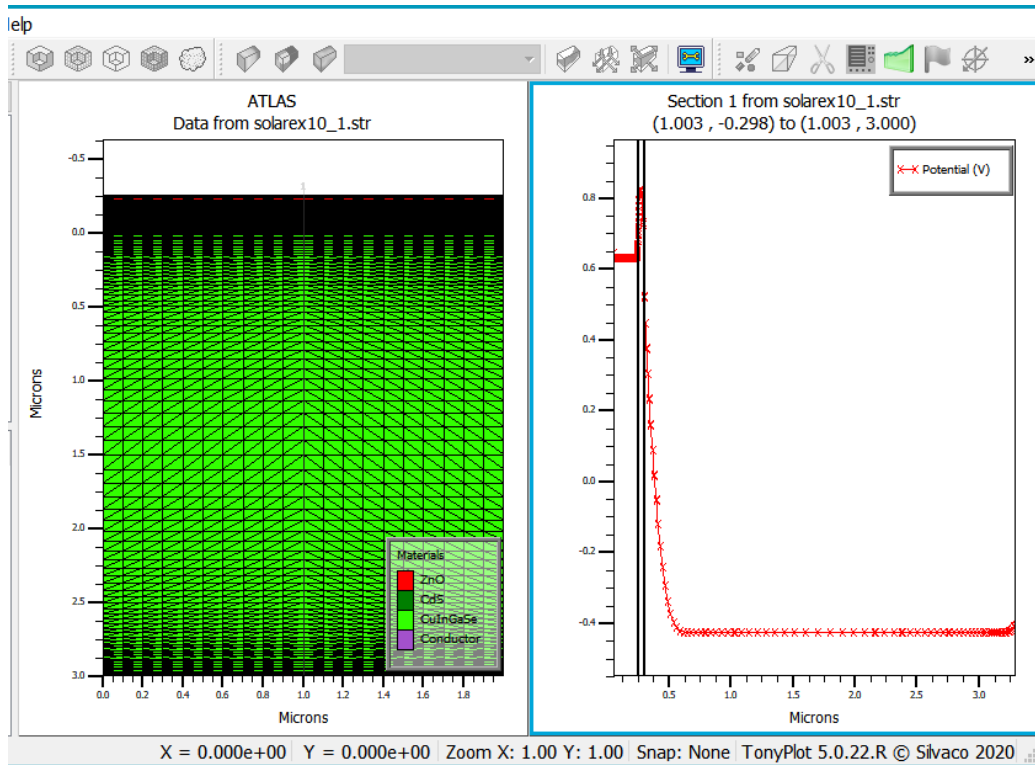
Figure IV.8: Electrical potential inside the CIGS-based solar cell at short-circuit condition and T=300°K.

Based on the calculation of the internal quantities, Silvaco-Atlas calculates the external quantities of the solar cell, such as the current density-voltage characteristics $(J - V)$ in the conditions of AM1.5standard solar spectrum.This is shown in figure IV.9 for the temperature T = 300°K. From the currentdensity -voltage characteristic $(J - V)$, it is possible to calculate the valuesof the photovoltaic parameters of the cell which are the short circuit current densityJ_{sc}, the open circuit voltage V_{oc}, the fill factor FF, the maximum power P_{max} provided from the cell and conversion efficiency η. Their values,corresponding to the ambient temperature T = 300°K,aregivenin figureIV.9.
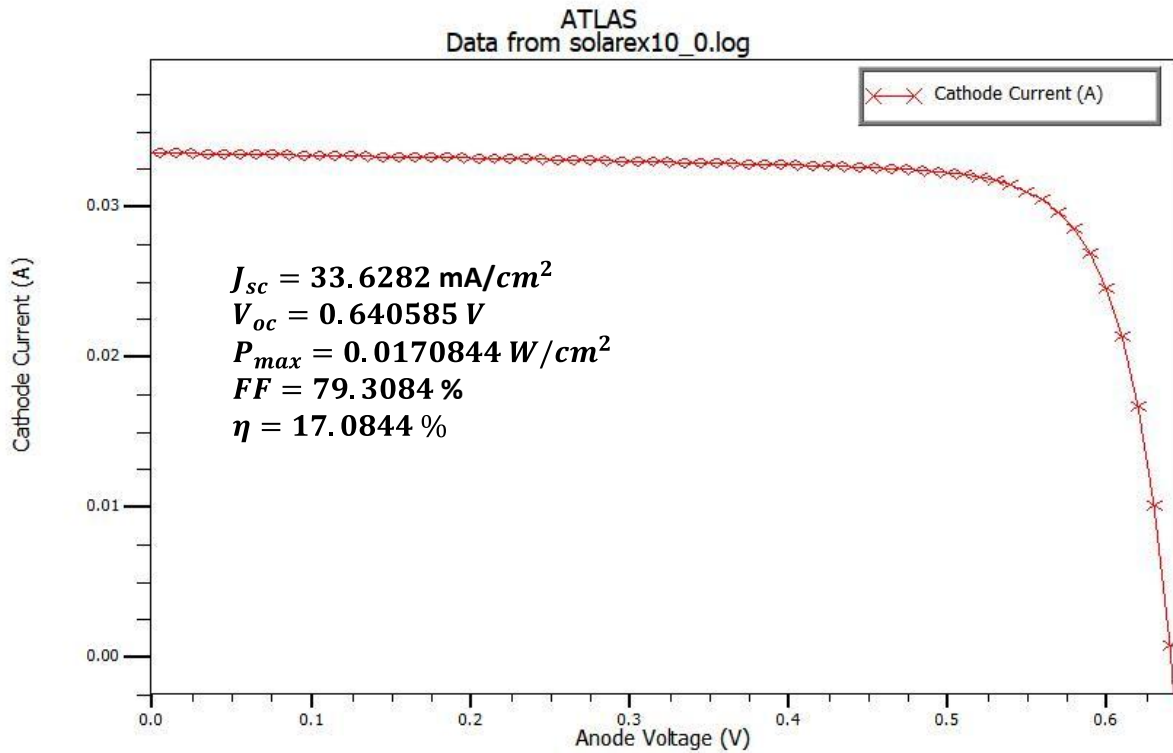
Figure IV.9: Current density-voltage $(J-V)$characteristic of the CIGS-based solar cell under the AM1.5 standard spectrum and T=300°K.

In the following we show the effect of temperature change in the range$[230°K-350°K]$ on some distribution of the internal quantities of the CIGS-based solar cell. Then, the temperatureeffectare shown on the external $J-V$and their photovoltaic parameters values.

Figures IV.10, IV.11 and IV.12 display, respectively,the band diagram, the distributions of electrons and holes concentration and the recombination rate in short circuit conditions for temperatures of 250°K, 300°K and 350°K within the range [230°K-300°K]. We notice, through these figures, that the temperature in general has a slight effect on the distribution of internal quantities.For example through figure IV.10, we notice a slight decrease in the potential barrier established between the two contacts of the n-type ZnO / n-type CdS / p-type CIGS junction through a slight decrease of both E_C and E_V in the p-type CIGS region as the temperature increased from 250°K to 350°K.This slight effect of temperature can be explained by the fact that the internal parameters are drawn it short circuit conditions where the electricalcurrent generated inside the cell is mainly a light (photo-) current and this latter is weakly affected by the temperature.
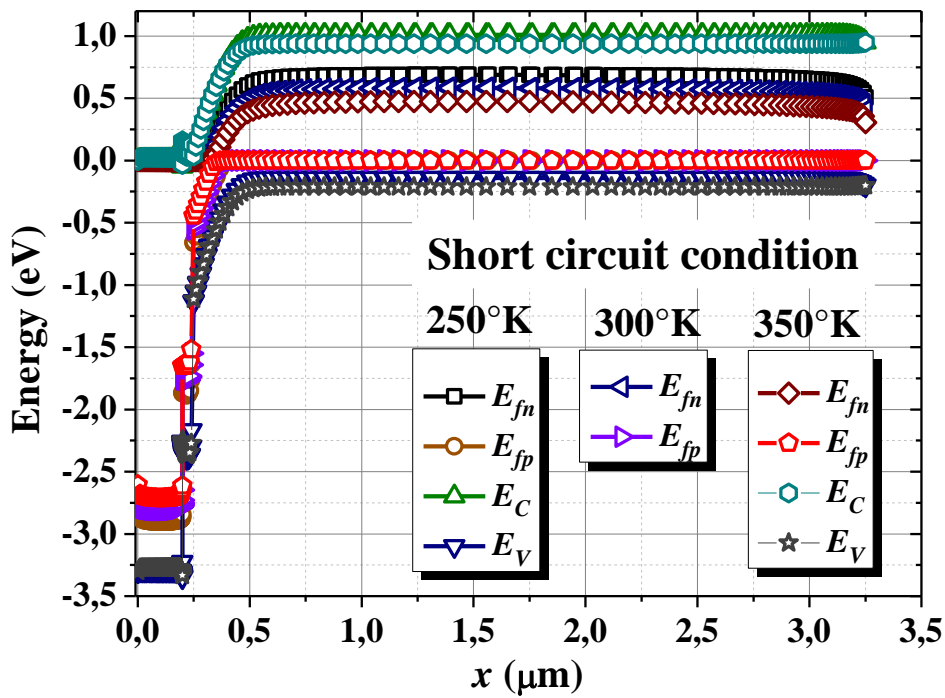
Figure IV.10: Band diagram of the CIGS-based solar cell at short-circuit condition for
T=250°K, T=300°K and T=350°K.
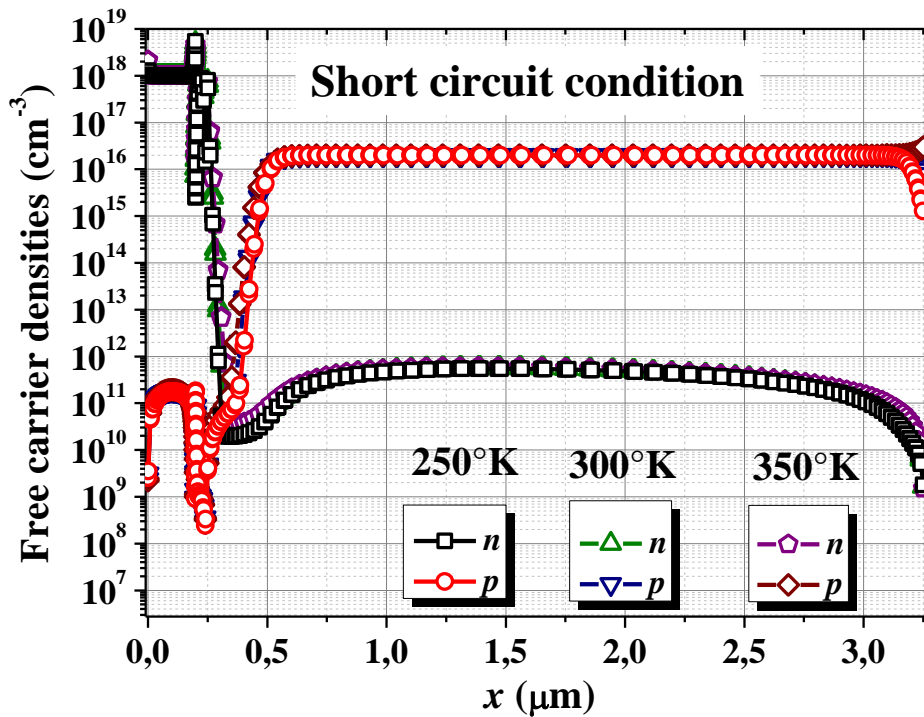
Figure IV.11: Free carrier densities in the CIGS-based solar cell at short-circuit
condition for T=250°K, T=300°K and T=350°K.
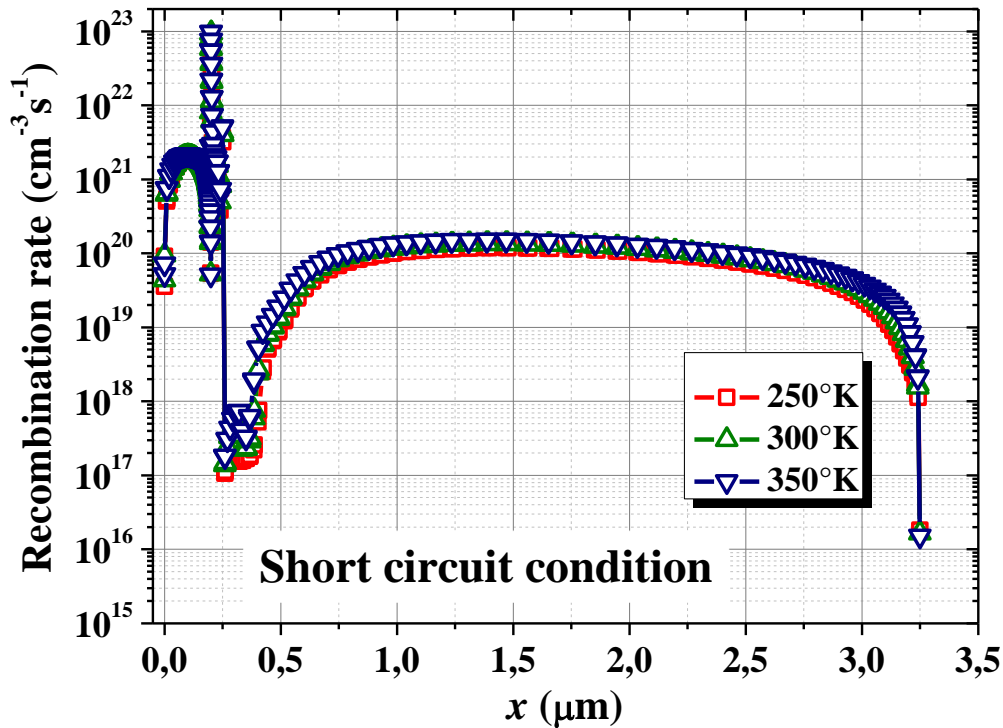
Figure IV.12: Recombination ratein the CIGS-based solar cell at short-circuit conditionfor
T=250°K, T=300°K and T=350°K.

We now turn to showing the effect of temperature on the external parameters of the
CIGS solar cell, which is the current density - voltage $(J - V)$characteristic shown in
figure IV.13 for temperatures of 250°K, 300°K and 350°K within the range [230°K-
350°K].Based on figureIV.13, we note that the prominent effect of temperature is on the
open circuit voltage V_{oc},the latter decreases noticeably with thetemperature increase from
250°K to 350°K. This leads directly to a decrease in both the fill factor FF and the
photovoltaic conversion efficiency η of the cell. The short circuit current densityJ_{sc},which
is essentially an optical (photo-) generated current, knowsotherwise aslight decrease with
temperatureincrease. The values of the photovoltaic parameters, represented by the short
circuit current density J_{sc}, the open circuit voltage V_{oc}, the fill factor FF, the maximum
power P_{max} delivered by the cell and the photovoltaic conversion efficiencyη of the cell,
areextracted from the current density-voltage $(J - V)$characteristic.They are listed in table
IV.3 under the effect of temperature increase in the range [230°K-350°K].
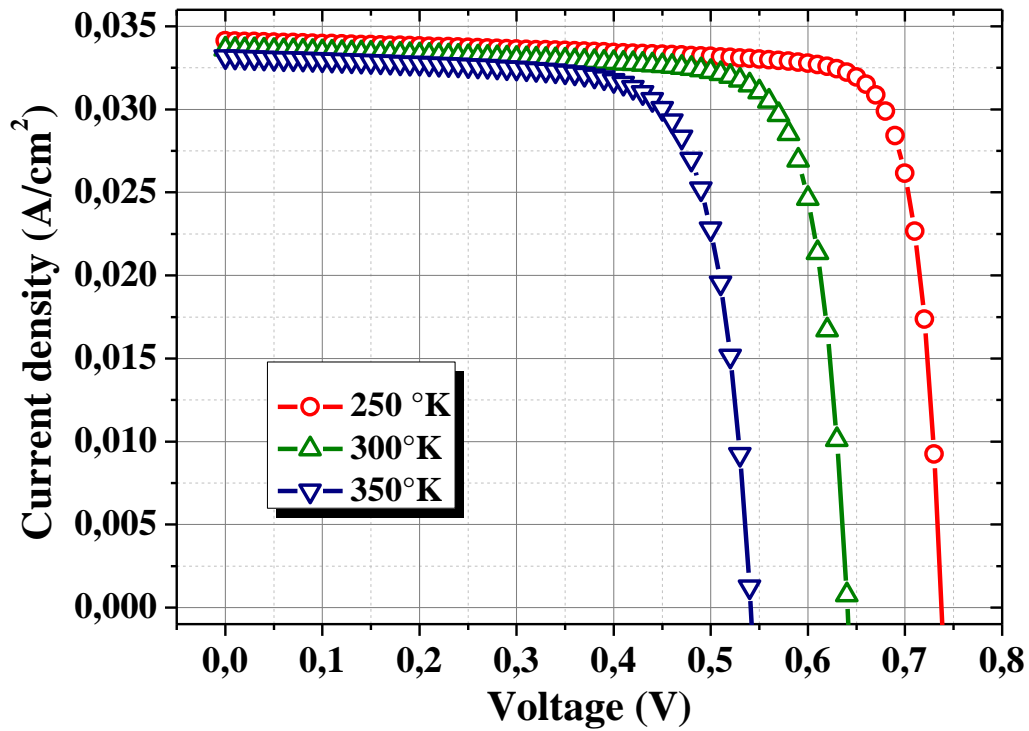
Figure IV.13: Current density-voltage $(J - V)$ characteristic of the CIGS-based solar cell
under the AM1.5 standard spectrum atT=250°K, T=300°K and T=350°K.

Table IV.3: Output photovoltaic parameters of the CIGS-based solar cell under the
temperature variation effect in the range $[230°K - 350°K]$.

Temperature (°K)	J_{sc} (mA/cm^2)	V_{oc} (V)	FF (%)	P_{max} (Watt/cm^2)	η (%)
230	34.3191	0.77551	83.8319	0.0223117	22.3117
250	34.1166	0.737525	82.6537	0.0207972	20.7972
270	33.9184	0.699162	81.3656	0.0192954	19.2954
290	33.724	0.660265	79.9954	0.0178124	17.8124
310	33.5332	0.620837	78.5877	0.0163609	16.3609
330	33.3466	0.581134	77.0376	0.014929	14.929
350	33.1659	0.541175	75.3297	0.0135206	13.5206

In addition, the variation of these photovoltaic parameters can be plotted,from table
IV.3, with temperature increase, as shown by figuresIV.14, IV.15, IV.16 and IV.17,
respectively, for the short circuit current density J_{sc}, the open circuit voltage V_{oc}, the fill
factorFF, and the photovoltaic conversion efficiencyη of the cell.
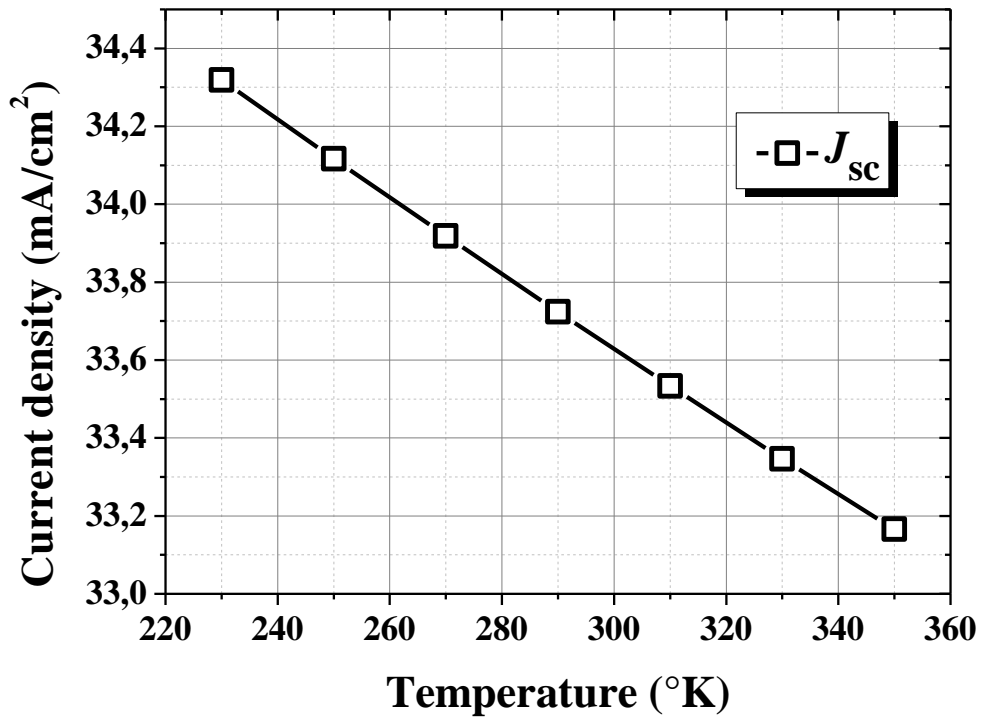
Figure IV.14: Temperature dependency of the short circuit current density (J_{sc}) of the CIGS-based solar cell under the AM1.5 standard spectrum.
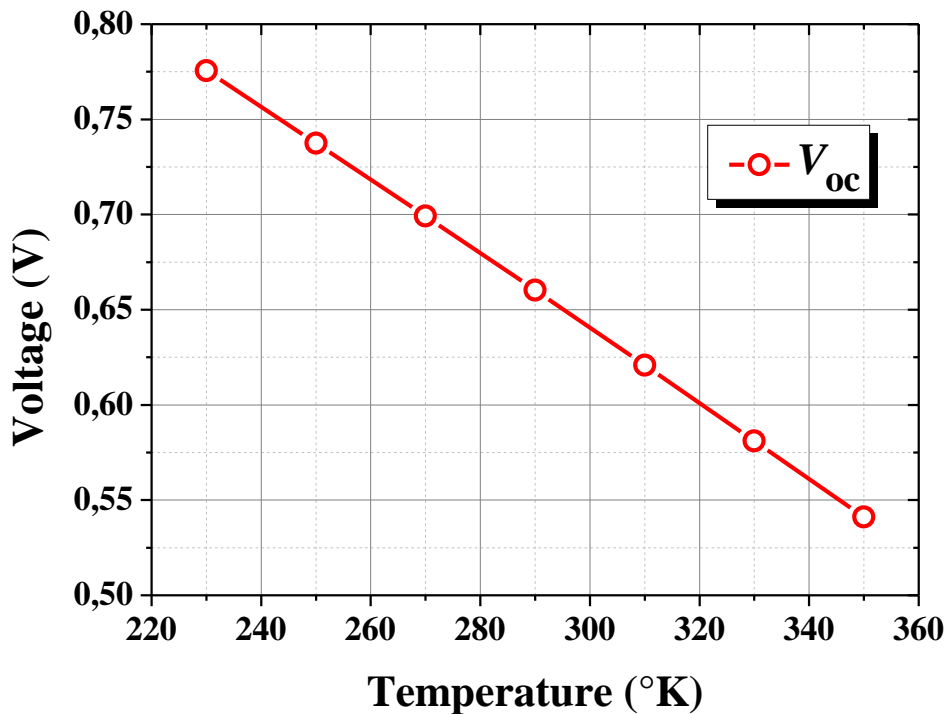
Figure IV.15: Temperature dependency of the open circuit voltage (V_{oc}) of the CIGS-based solar cell under the AM1.5 standard spectrum.

Figure IV.16: Temperature dependency of the fill factor (*FF*) of the CIGS-based solar cell
under the AM1.5 standard spectrum.
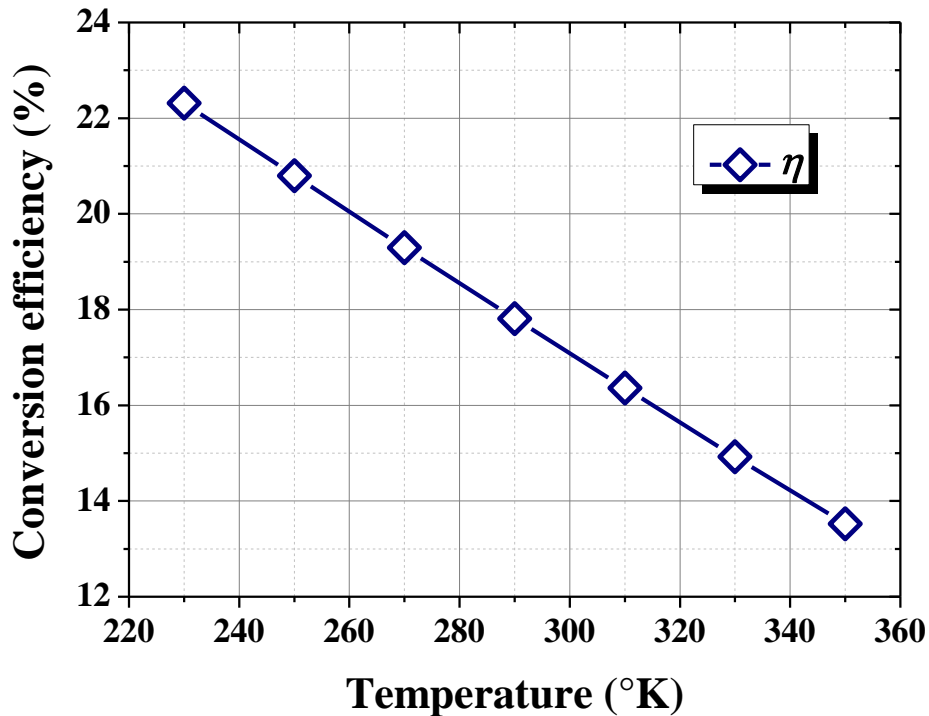
Figure IV.17: Temperature dependency of the conversion efficiency (η) of the CIGS-
based solar cell under the AM1.5 standard spectrum.

Chapter IV: temperature effect on the performance of Cu(In,Ga)Se$_2$ (CIGS)-based solar cell

Through the figuresIV.14, IV.15, IV.16 and IV.17, we can notifythe prominent temperature effect on the open circuit voltage V_{oc}.The latter decreases significantly with temperature increase in the range [230°K-350°K]. This leads directly to a decrease of both the fillfactor *FF* and the photovoltaic conversion efficiency$\eta$of the solar cell.

The open circuit voltage V_{oc} decrease with increasing temperature can be explained by the well-known theoretical equations relatingV_{oc} to both the short circuit current density J_{sc} and the saturation current density J_s.

For the example of the ideal case, where we neglect the effect of both series resistance and parallel resistance, the characteristic of the currentdensity -voltage of the solar cell is written as follows:

$$J(V) = J_{ph} - J_s \left[exp \left(\frac{qV}{nk_BT} \right) - 1 \right] \tag{IV.1}$$

Where V is the voltage between the two contacts of the cell, J_{ph} is the density of the optically generated current inside the cell and n is the idealityfactor (or quality factor)of the solar cell which takes values in the range [1-2].

Considering $J_{sc} \cong J_{ph}$ and considering the open circuit conditions($V = V_{oc}$), the total current is zero $(J(V) = 0)$ and then:

$$J_{sc} - J_s \left[exp \left(\frac{qV_{oc}}{nk_BT} \right) - 1 \right] = 0 \tag{IV.2}$$

So:

$$V_{OC} = \frac{nk_BT}{q} ln \left(\frac{J_{sc}}{J_s} + 1 \right) \tag{IV.3}$$

We know that the J_s saturation current of the cell is thermally activated, that is, it increases with increasing temperature because:

$$J_s = q. \left[\frac{L_P}{\tau_P N_d} + \frac{L_n}{\tau_n N_a} \right] n_i^2 \tag{IV.4}$$

$$J_s = q. \left[\frac{L_P}{\tau_P N_d} + \frac{L_n}{\tau_n N_a} \right].4 \left(\frac{2\pi k_B T}{h^2} \right)^3 (m_e^* m_t^*)^{3/2}. exp \left(-\frac{E_g}{k_BT} \right) \tag{IV.5}$$

Where n_i the intrinsic concentration, L_p and L_n are the diffusion lengths of holes and electrons, τ_P and τ_n are the life time of holes and electrons, N_d and N_a are the doping concentrations of the donor and acceptor atoms, m_e^* and m_t^* are the effective masses of the electrons and holes.

So the saturation current J_s increases with increasing temperature, and because J_{sc} is slightly affected by temperature, sothe V_{oc} decreases with increasing temperature through equation (IV.3). On the other hand, decreasing V_{oc} with increasing temperature leads to a direct and noticeable decrease in the fill factor FF, and there is an experimental formula that demonstrates this through experimental work of the references [30-31-32] :

$$FF = \frac{v_{OC} - ln(v_{OC} + 0.72)}{v_{OC} + 1} \tag{IV.6}$$

Where$v_{OC} = \frac{q.V_{OC}}{n.k_B T}$.

Decreasing both ofV_{oc} and FF leads to a decrease in the photovoltaic conversion efficiency, as shown in table IV.3 and figure IV.17.

The rate of decrease of the short circuit current density J_{sc}, the open circuit voltage V_{oc}, the fill factor FF, and the conversion efficiencyη of the photovoltaic cell, with increasing temperature, is shown in table IV.4.

Table IV.4: Reduction rate ofJ_{SC}, V_{OC} , FFandη with ambient temperature (°C) increase of the (n-type ZnO/n-typeCdS/p-typeCIGS) solar cell.

$\frac{\Delta J_{SC}}{\Delta T}\left(\frac{mA}{cm^2 \cdot C}\right)$	$\frac{\Delta V_{OC}}{\Delta T}\left(\frac{V}{\cdot C}\right)$	$\frac{\Delta FF}{\Delta T}\left(\frac{\%}{\cdot C}\right)$	$\frac{\Delta \eta}{\Delta T}\left(\frac{\%}{\cdot C}\right)$
$\cong -9.614 \times 10^{-3}$	-0.001952	-0.07085	-0.07325

I.V.Conclusion:

In this work, we have studied the performance of a Cu(In,Ga)Se_2 (CIGS) –based solar cell using SILVACO-ATLAS numerical simulation software. This latter allowed the computation of all internal parameters distributions of the solar cell such as the band diagram distribution, electron and hole concentrations, the recombination rate, as well as

the external parameters such as the current density-voltage $(J - V)$ characteristic, from which we have extracted the values of the output photovoltaic parameters characterising the solar cell performance which are the short circuit current density J_{SC}, the open circuit voltage V_{OC}, the fill factor FF, the maximum power P_{max} provided by the cell and the photovoltaic conversion efficiency η of the cell. In this work, we have studied the ambient temperature effect on the performance of the solar cell exposed to the AM1.5 standard spectrum in terms of the effect on both internal and external parameters. The considered temperature range is [230°K-350°K] equivalent to [(-43°C)-(77°C)].

The obtained results from this study lead to the following conclusions:

-The temperature, in general, has a slight effect on the distribution of the internal parameters of the solar cell when calculating these latter under short-circuit condition. We explained that by the fact that the electrical current generated inside the cell is, in these conditions, mainly a photo-current which is weakly affected by the temperature.

- The noticeable temperature effect of on the open circuit voltage V_{OC}. Indeed, this latter decreases significantly with temperature increase in the range [230°K-350°K]. This leads directly to the fill factor (FF) decrease, and consequently, the decrease of the photovoltaic conversion efficiency η of the cell from 22.31% for 230°K to 13.52% for 350°K. The open circuit voltage (V_{OC}) decrease, with temperature increase, was explained by the known theoretical equations relating V_{OC} to both the short circuit current density J_{SC} and the saturation current density J_S.

General conclusion

Solar cells are required for efficient, cost-effective, andhighly proficient conversion of sunlight to electrical energyat low cost. Current energy needs worldwide indicate therequirement for cost-effective, efficient power conversionusing copper indium gallium diselenide(Cu(In,Ga)Se$_2$,CIGS)-based thin-film solar cells. The conversionefficiency of CIGS solar cells is sufficiently high (~17% - 23%), whiletheir outdoor performance is admirable. Moreover, thischalcogenide material represents a perfect candidate materialfor the p-type absorber layer in CIGS-based solar cells. Although CIGS suffers from high manufacturing cost,it provides better performance than other thin-film solar celltechnologies such as CdTe or a-Si:H. This high cost isdue to the use of the rare metals gallium (Ga) and indium(In). Due to their scarcity, the CIGS layer should be as thinas possible, to minimize the cost of the absorber material.

In this work, we haves studied the performance of a Cu(In,Ga)Se_2 (CIGS) –based solar cell using SILVACO-ATLAS numerical simulation software.This latter allowed thecomputation of all internal parametersdistributions of the solar cell such as the band diagram distribution, electron and hole concentrations, the recombination rate, as well as the external parameters such as the current density-voltage $(J - V)$ characteristic, from which we haveextracted the values of theoutput photovoltaic parameters characterising the solar cell performance which are the short circuit current density J_{SC}, the open circuit voltage V_{OC}, the fill factor FF, the maximum powerP_{max} provided by the cell and the photovoltaic conversion efficiency η of the cell. In this work, we have studied the ambient temperature effect on the performance of the solar cell exposed to theAM1.5 standard spectrum in terms of the effect on both internal and external parameters. The considered temperature range is [230°K-350°K] equivalent to [(-43°C)-(77°C)].

The obtained results from this study lead to the following conclusions:

-The temperature, in general, has a slight effect on the distribution of the internal parameters of the solar cell when calculating these latter under short-circuit condition.Weexplained that by the fact that the electrical current generated inside the cell is, in these conditions, mainly a photo-current which is weakly affected by temperature.

-The noticeable temperature effect of on the open circuit voltage V_{OC}.Indeed, this latter decreases significantly with temperature increase in the range [230°K-350°K].This leads directly to the fill factor (FF) decrease, and consequently,the decrease of the photovoltaic

conversion efficiency η of the cell from 22.31% for 230°K to 13.52% for 350°K. The open circuit voltage (V_{OC}) decrease, with temperature increase, was explainedby the known theoretical equations relating V_{OC} to both the short circuit current density J_{SC} and the saturation current density J_S.

As perspective, we will investigate a comparative study between a solar cell based on mono-crystalline CIGS and other based on polycrystalline CIGS under the influence of both ambient temperature and light intensity.

References

[1] M. Iqbal, An Introduction to Solar Radiation. New York, NY: Academic Press, 2012.

[2] B. Richards, "Enhancing the performance of silicon solar cells via the application of passive luminescence conversion layers," Solar Energy Mater.Solar Cells, vol. 90, pp. 2329–2337, 2006.

[3] S. M. Sze and M. K. Lee, Semiconductor Devices: Physics and Technology. 3rd ed. New York, NY: John Wiley & Sons, 2012.

[4] M. Zeman, Solar Cells. 1st ed. Delft, Netherlands: Delft University of Technology, 2005.

[5] Module IV curve (n.d.). Folsom Labs [Online] Available: https://www.folsomlabs.com/modeling/module/module_model Accessed August 3, 2015.

[6] A. Luque and S. Hegedus, Handbook of Photovoltaic Science and Engineering.3rd ed., West Sussex, United Kingdom: John Wiley & Sons, 2011.

[7] S. R. Wenham," Cell Properties and Design" in Applied Photovoltaics.3rd ed., New York, NY: Earthscan, 2011, pp. 55–65.

[8] C. S. Solanki, Photovoltaic technology and systems. 1st ed., Delhi, India: PHI Learning Private Limited, 2013.

[9] T. Ghorbani, M. Zahedifar, M. Moradi, E. Ganbari, "*Influence of affinity band gap ambient temperature on the efficiency of CIGS solar cells*", ELSEVIER, volume 223, December 2020, 165541.

[10] Chen. Wang, DamingZhuang, Ming Yaouei Wei, XunyanLyu, GuoanRen, Yixuan Wu, LanHu, Yuxian, Qianming Gong, Jinquan Wei, "*The effects of preheating temperature on $CuInGaSe_2/CdS$ interface and the device performances*", volume 194, December 2019, Page11-17.

[11] M. A. Green, Y. Hishikawa, E. D. Dunlop, D. H. Levi, J. Hohl-Ebinger, and A. W. Y. Ho-Baillie, "Solar cell efficiency tables (version 52),"Progress in Photovoltaics: Research and Applications, vol. 26, no. 7, pp. 427-436, 2018.

[12] G. Kavlak, J. McNerney, and J. E. Trancik, "Evaluating the causes of cost reduction in photovoltaic modules,"Energy Policy, vol. 123, pp. 700-710, 2018.

[13] T. D. Lee and A. U. Ebong, "A review of thin film solar cell technologies and challenges,"Renewable and Sustainable Energy Reviews, vol. 70, pp. 1286-1297, 2017.

[14]SSandeep *"General Structure of Solar Cells"* March 2011. (Accessed Dec. 9th **2011**). http://www.ncpre.iitb.ac.in/page.php?pageid=54&pgtitle=Si-Solar-Cells.

[15] S Chen, J-H Yang, XG Gong, A Walsh, and S-H. Wei. "Intrinsic point defects and complexes in the quaternary kesterite semiconductor Cu2ZnSnS4".Phys. Rev. B 81; 245204 (1-10); 2010.

[16] I Repins, N Vora, C Beall, S-H Wei, Y Yan, M Romero, G Teeter, H Du, B To, M Young, M Noufi. "Kesterites and Chalcopyrites: A Comparison of Close Cousins". NREL Preprint, Presented at the Materials Research Society Spring Meeting 2011.

[17] NREL: Best Research Cell Efficiencies. http://www.nrel.gov/ncpv/images/efficiency_chart.jpg. (Accessed Dec. 9th **2011**).

[18] A. Chirilă, S. Buecheler, F. Pianezzi, P. Bloesch, C. Gretener, A. R. Uhl, C. Fella, L. Kranz, J. Perrenoud and S. Seyrling, "Highly efficient Cu (In, Ga) Se2 solar cells grown on flexible polymer films," Nature Materials, vol. 10, no. 11, pp. 857–861, 2011.

[19] X. Ma, D. Liu, L. Yang, S. Zuo and M. Zhou, "Molybdenum (mo) back contacts for CIGS solar cells," in Eighth Int. Conf. on Thin Film Physics and Applications, 2013, pp. 906814-906814.

[20] M. A. Green, K. Emery, Y. Hishikawa, W. Warta and E. D. Dunlop, "Solar cell efficiency tables (Version 45)," Progress in Photovoltaics Research Applications, vol. 23, no 1, pp. 1–9, Jan., 2015.

[21] R. L. Garris, J. V. Li, M. A. Contreras, K. Ramanathan, L. M. Mansfield, B. Egaas and A. Kanevce, "Efficient and stable CIGS solar cells with ZnOS buffer layer," in Photovoltaic Specialist Conference, 2014, pp. 0353–0356.

[22] R. L. Garris, J. V. Li, M. A. Contreras, K. Ramanathan, L. M. Mansfield, B. Egaas and A. Kanevce, "Efficient and stable CIGS solar cells with ZnOS buffer layer," in *Photovoltaic Specialist Conference,* 2014, pp. 0353–0356.

[23] G. Hanna, A. Jasenek, U. Rau and H. Schock, "Influence of the Ga-content on the bulk defect densities of Cu (In, Ga) Se 2," Thin Solid Films, vol. 387, no. 1, pp. 71–73, May 2001.

[24] S. Song, K. Nagaich, E. Aydil, R. Feist, R. Haley and S. Campbell, "Structure optimization for a high efficiency CIGS solar cell," in Photovoltaic Specialists Conference (PVSC), 2010, pp. 2488–2492.

[25] L. Kerr, S. Li, T. Anderson, O. Crisalle, S. Johnston, J. Abushama and R. Noufi, "DLTS characterization of CIGS cells," in NCPV and Solar Program Review Meeting Proceedings, Golden, CO, 2003, pp. 866-869.

[26] Su-Huai Wei, S.B. Zhang, and Alex Zunger. Effects of Na on the Electrical and Structural Properties of CuInSe2. Journal of Applied Physics, 85(10):7214–7218, May 1999.

[27] S.M. Sze and Kwok K. Ng. Physics of Semiconductor Devices.Wiley-interscience, 2007.

[28] Markus Gloeckler. Device Physics of Cu(In,Ga)Se2 Thin-Film Solar Cells. PhD thesis, Colorado State University, 2005.

[29] ATLAS User's Manual, vols. 1–2, software version 5.6.0.R, Silvaco International, Santa Clara, CA, 2012.

[30] http://www.pveducation.org/pvcdrom

[31]M.A. Green, Solar cell fill factors: General graph and empirical expressions, Solid-State Electronics Vol. 24, No. 8, pp. 788 - 789, 1981.

[32]P. Singh, N.M. Ravindra, Temperature dependence of solar cell performance—an analysis, Solar Energy Materials & Solar Cells 101 (2012) 36–45.

Abstract

In this work, we havestudied a Cu(In, Ga)Se_2 (CIGS) –based solar cell under the effect of the ambient temperature change in the range of [230°K-350°K]. The cell is exposed to theAM1.5 standard spectrum, and its performance was simulatedbySILVACO-ATLAS software, which allowed the calculation of both the internal and external parameters. These latter arerepresented by the currentdensity-voltage $(J - V)$ characteristic, from which wehave extracted the output photovoltaic parameterscharacterisingthe cell performance. The temperature, in general, has a slight effect on the internal parameterdistributions of the solar cell when these latter are calculatedunder the short circuit conditions.However, the temperature has a noticeable effect on the open circuit voltage V_{OC} which decreases significantly with temperature increase in the range [230°K-350°K]. This leads directly to the decrease of the fill factor FF, and consequently the decrease of the photovoltaic conversion efficiency $\eta$from 22.31% for 230°K to 13.52% for350°K.

ملخص

في هذا العمل درسنا عن طريق محاكاةخلية شمسية من مادة (CIGS)Cu(InGa)Se_2

تأثير تغيير درجة الحرارة المحيطة في المجال   [230°k-350°k]   على اداء الخليةالمعرضة للإشعاع الشمسي المعياري AM1.5. حيث استخدما برنامج المحاكاة الرقمية   SILVACO-ATLAS والذي سمح بحساب كل من الوسائط الداخلية وكذلك الخارجية المتمثلة في الخاصية كثافة التيار-جهد التي استخلصنا منها الوسائط الفوطوفولطائية المميزة لأداء هذه الخلية.

لدرجة الحرارة على العموم تأثير طفيف على توزيعة المقادير الداخلية للخليةعند حساب هذه الأخيرة في شروط الدارة القصيرة . في حيناتضح التأثير البارز لدرجة الحرارة على جهد الدارة المفتوحة V_{OC}الذي يتناقص تناقصا ملحوظا مع زيادة درجة الحرارة في المجال[$350°K − 230°K$]. و هذا ما أدى بشكل مباشر إلى نقصان معامل التعبئة FF ، و بالتالي نقصان نقصان مردود التحويل الفوطوفولطائي للخلية η من 22.31% بالنسبة لدرجة الحرارة $230°K$ إلى 13.52% بالنسبة لدرجة الحرارة $350°K$.